UNIVERSITY OF OKLAHOMA

GRADUATE COLLEGE

INTERFACE EQUILIBRATION PROCESSES AND THEIR EFFECTS ON WETTABILITY AND INTERFACIAL ENERGY

A DISSERTATION

SUBMITTED TO THE GRADUATE FACULTY

in partial fulfillment of the requirements for the

Degree of

DOCTOR OF PHILOSOPHY

By

ORPHIUS ISLAM MOHAMMAD
Norman, Oklahoma
2009

INTERFACE EQUILIBRATION PROCESSES AND
THEIR EFFECTS ON WETTABILITY AND INTERFACIAL ENERGY

A DISSERTATION APPROVED FOR THE
SCHOOL OF CIVIL ENGINEERING AND ENVIRONMENTAL SCIENCE

BY

_____
Dr. Tohren C. G. Kibbey, Chair

_____
Dr. David A. Sabatini

_____
Dr. Randall L. Kolar

_____
Dr. K.K. (Muralee) Muraleetharan

_____
Dr. Edgar A. O'Rear III

ACKNOWLEDGEMENTS

First of all, I want to express my deep and sincere gratitude to the omniscient Allah (God almighty) for allowing me to bring this effort to success.

I would like to express my worm and sincere thanks to my advisor, Dr. Tohren C. G. Kibbey, for every thing he did for me throughout my study in University of Oklahoma. I am very grateful to him for his guidance and sound advice in every aspects of my study. This work would not have been possible without his teaching, guidance, and good ideas that help me to keep pursuing my goal. He was always patient and supportive in my bad time and gave me all sorts of help and encouragement to keep going with my research work.

I would like to thank my committee members: Dr. David A. Sabatini, Dr. Randall L. Kolar, Dr. K.K. (Muralee) Muraleetharan and Dr. Edgar A. O'Rear III for their time and interest in my research work. Their valuable suggestion and advice help me to complete this dissertation.

I would like to use this opportunity to thank my mother: Halida Edib and my father: Md. Nazrul Islam back in Bangladesh. Their unconditional love and guidance always inspire me to be a better person in my life.

And at last but not least, I want to thank my wife: Shejuti Silvia and my 11 month old son: Aayan Zarif for their love, comfort and support throughout my life. With out my wife's unconditional support and love, I would not be able to come even close to finish my research work. At the end of a very tiring and stressful day, when I look at my son or sit by my wife, I forget all my stresses and feel reenergize for the next day.

TABLE OF CONTENTS

LIST OF TABLES

LIST OF FIGURES

ABSTRACT

Surface/interface equilibration and wettability modification of organic liquids are two important phenomena in many practical applications including subsurface remediation, detergency and food industry. Although surface/interface equilibration and wettability are two different processes, they are closely related to each other when applied to organic liquids. The objective of this research work is to study the dynamics of surface equilibration process of organic liquids and its implication on the change of wettability.

Because of their low aqueous solubilities, dense nonaqueous phase liquids (DNAPLs) persist as long-term sources of contamination. Although natural dissolution can occur slowly, because it occurs at DNAPL-water interfaces, it may influence the wettability of aquifer materials in the presence of DNAPLs. The wettability of aquifer materials and properties of DNAPL-water interfaces can influence how DNAPLs infiltrate through the subsurface, and how easily they can be remediated.

Surfactants are widely used in subsurface remediation, detergency, oil recovery, pharmaceutical industry and food industry. Surfactant monomer adsorbs on the surface or interface. When surfactant adsorbs, surface/interfacial tension initially is not equal to equilibrium interfacial tension of the system. Depending on the fluid types, phase volumes, concentration and interfacial area it may take milliseconds to days to attain equilibrium surface/interfacial tension. So for different practical applications, it is very important to understand the adsorption kinetics of surfactant and the corresponding effect on dynamic surface/interfacial tension over time.

This research work examines the dynamics of surface/interface equilibration of organic liquids and its effect on wettability modification. The study has been accomplished by three different types of experiments: (i) Dissolution of DNAPLs (sessile drop) in water (in presence and absence of surfactant), (ii) Dilution of different types (cationic, anionic and nonionic) of surfactant solution (dilution of surfactant pendent drop in air by injecting water into the drop) and (iii) Evaporation of surfactant solution (pendent drop in air). Considering the experimental result, numerical models have been developed to understand the surface/interface equilibration phenomena and its effect on wettability modification.

The result of this study will provide a better understanding of surface/interface equilibration phenomena of organic liquids and their effects on wettability modification.

CHAPTER 1

INTRODUCTION

Surfactant adsorption at surfaces or interfaces is an important phenomenon in many different practical applications such as oil recovery, pharmaceutical industries, subsurface remediation and detergency (1). When a system consists of two immiscible phases, the boundary between the phases is known as an interface. When one of the phases is gas, the boundary between the phases is known as a surface (2, 3). The surface/interfacial free energy is the minimum amount of work per unit area required to create that surface/interface and surface/interfacial tension is the force per unit length of the surface or interface required to stretch the surface/interface (2, 4, 5).

When surfactant monomer first adsorbs on the surface or interface, the interfacial tension, γ, is not equal to the equilibrium interfacial tension, γ_{eq}. Because of the concentration gradient of surfactant monomer between the bulk phase and the surface/interface, surfactant monomer continues to adsorb on the surface/interface. Over time the concentration of surfactant monomer at surface/interface reaches a dynamic equilibrium (the rate at which monomer arrives at the surface/interface is equal to the rate at which monomer leaves the surface/interface) and surface/interfacial tension (γ) equals the equilibrium surface/interfacial tension (γ_{eq}) (6, 7, 8).

Dynamic surface/interfacial tension ($\gamma(t)$), is a very important measurement for understanding adsorption of surfactant. There are various techniques available for

measuring dynamic surface/interfacial tension including maximum bubble pressure method (9), drop volume method (10), pendent drop method (11, 12, 13).

Various adsorption models have been developed to describe dynamic surface tension and adsorption phenomena of surfactant. The work by Ward and Tordai is considered as pioneering in this field of study. In 1946 they first published a mathematical analysis for surfactant adsorption by using a diffusion-controlled model (14). Their model accounts for diffusion of surfactant monomer from bulk phase to interface, and also "back-diffusion" of surfactant monomer from interface to bulk phase when the interface becomes over-crowded (14). Later numerous theoretical and numerical studies were published to improve the model given by Ward and Tordai (e.g., (7, 15, 16)).

In these adsorption models, either a pendent drop of surfactant solution is formed in the air by using a syringe (7) or air bubble is formed in surfactant solution (16) and that surfactant drop or air bubble is held for some time period to observe surfactant adsorption on surface or interface. So these models address only static condition of surfactant solution. But in practical applications, such as ground water remediation, surfactant solution mix with ground water and undergoes continuous change of concentration. This change of concentration may lead to a change of interfacial tension of surfactant. These models do not address these dynamic conditions (change of concentration and interfacial tension with time). As a part of this work, experiments were designed to examine the effects of dilution and evaporation on surface/interface equilibration of surfactant (adsorption of surfactant at surface/interface and its effect on surface/interfacial energy modification).

When two immiscible fluids contact a solid surface, the angle between the fluid-fluid interface and the solid surface is referred to as the contact angle (17).

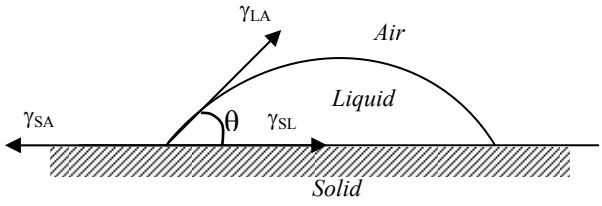

Figure 1.1 Contact angle in a solid-liquid-air system. (θ: contact angle, γ_{LA}: surface tension between liquid and air, γ_{SA}: surface tension between solid and air, γ_{SL}: interfacial tension between solid and liquid.)

The fluid through which the contact angle is less than 90 degrees is said to be the wetting fluid (17). So wettability can be described from the magnitude of contact angle. Contact angles are influenced by changes in surface/interfacial tension and can be described by Young's equation (4):

$$\cos\theta = \frac{\gamma_{SA} - \gamma_{SL}}{\gamma_{LA}} \qquad (1.1)$$

Where, θ: contact angle,

γ_{LA}: surface tension between liquid and air,

γ_{SA}: surface tension between solid and air and

γ_{SL}: interfacial tension between solid and liquid.

Change in surface/interfacial tension values can result in changing contact angle. So interfacial energy modification can also affect ground water contamination by changing wettability of entrapped organic liquid.

Chlorinated solvents are typically non-flammable and are widely used in industrial facilities (18). Chlorinated solvents are typically higher in density than water, have low aqueous solubilities and are often referred to as dense nonaqueous phase liquids (DNAPLs). Because of their low aqueous solubilities, DNAPLs persist as long-term sources of contamination. Subsurface contamination by DNAPLs, such as chlorinated solvents, can be observed in industrial areas through out the world (19, 20, 21, 22).

Because of their low solubilities in water and high densities, when DNAPLs enter the subsurface by means of spills or leaks, they form a separate phase, which may move downward through the vadose zone, penetrate the water table and remain in the aquifer for a long time (23). The ultimate distribution of DNAPLs in the subsurface is influenced by a number of factors, including the interfacial tension between the DNAPL and water, and the contact angle between the two fluids and the soil surfaces (24, 25).

The effect of pH, ionic strength and solutes of solution on contact angle modification has been studied (26, 27, 28, 29, 30, 31), but the effect of dissolution of DNAPLs on dynamic contact angle has not yet been reported. The focus of the work was to examine the change of wettability (contact angle) and interfacial energy of DNAPLs under the influence of dissolution in water in presence and absence of surfactant.

CHAPTER 2

CONTACT ANGLE AND WETTABILITY

2.1. INTRODUCTION

The contact angle of DNAPL in water at aquifer material interfaces influences the spatial distribution of DNAPLs as they infiltrate into the aquifer, and may ultimately influence their remediation. The work described in this chapter examines the influence of dissolution in water of two chlorinated organic liquids, trichloroethylene (TCE) and tetrachloroethylene (PCE), on their contact angles on glass surfaces. When a drop is formed on a surface, and then the drop volume is gradually reduced (e.g., with a syringe), the base of the drop often maintains its initial footprint, and the contact line (where the two fluids and the solid meet) remains pinned until the contact angle reaches the receding angle. As the drop volume continues to decrease, the drop footprint will begin to shrink. Because dissolution causes drop volume to decrease, this same behavior is expected to be observed. Although the effects of solution properties (pH, ionic strength, solutes) on contact angles have been widely studied (e.g., 26-31), the effect of dissolution of DNAPLs on contact angles has not been previously reported.

2.1.1. *Dense Nonaqueous Phase Liquid*

The chlorinated organic liquids are typically nonflammable and are widely used in industrial applications (18). The chlorinated organic liquids are tend to be higher in

density than that of water, and they are typically immiscible with water. Because of high density and low aqueous solubility, many chlorinated organic liquids are considered as dense nonaqueous phase liquids (DNAPLs).

Because of their high densities, DNAPLs tend to migrate downward in aquifers and accumulate at underlying low-permeability layers. Because of their low aqueous solubilities, DNAPLs can persist as long-term sources of contamination. Subsurface contamination by DNAPLs such as chlorinated organic liquids is an extensive problem at contaminated sites around the world (19, 20, 21, 22).

2.1.2. *Contact Angle and Wettability*

As DNAPLs infiltrate into the subsurface, both the rate at which they infiltrate and their ultimate configuration are influenced by a number of factors, including the interfacial tension between the DNAPL and water, and the contact angle between the two fluids and the solid surfaces (24, 25). When two immiscible liquids come into contact with a solid surface, the angle between the liquid-liquid interface and the solid surface is known as contact angle **(**17**)**. In Figure 2.1, TCE (trichloroethylene) and water are the two immiscible liquids and 'θ' refers to the contact angle through water. The liquid through which the contact angle is less than 90^0 is known as wetting fluid (17). In Figure-2.1 water is the wetting fluid and TCE is the non-wetting fluid. So wettability of DNAPLs (dense non aqueous phase liquids) can be defined by the magnitude of contact angle.

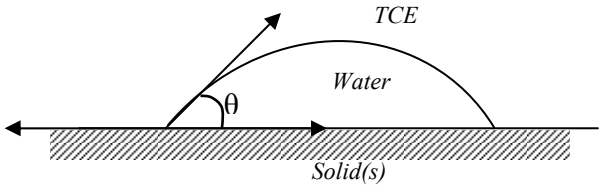

Figure 2.1 Contact angle in a solid-liquid-liquid system. (TCE: non-wetting fluid, water: wetting fluid, θ: contact angle)

For a relatively clean DNAPL infiltrating into a saturated sandy aquifer, water will generally be the wetting fluid (24). The nonwetting fluid, DNAPL, has to displace water from pores to infiltrate into the aquifer. The lower the contact angle through the water in the presence of the DNAPL, or the higher the interfacial tension between the two phases, the more strongly the water will resist being displaced from pores. For relatively small DNAPL spills, the DNAPL will ultimately be dispersed until it is in the form of disconnected droplets or blobs at a nonwetting phase saturation known as the residual nonwetting phase saturation (17). Larger spills may also become pooled on low permeability formations (23, 32).

Although wettability can be defined by the magnitude of the contact angle, that definition is complicated by the fact that contact angle is hysteretic, having different values depending on whether a fluid is advancing or receding over a surface (4, 5). The angle formed when liquid moves out over a new surface is known as the advancing contact angle (θ_A), and the angle formed when liquid moves off of a previously occupied surface is known as the receding contact angle (θ_R) (Figure 2.2). Receding contact angles are typically smaller than advancing contact angles (4, 5). And the difference between advancing and receding contact angle is known as contact angle hysteresis (4).

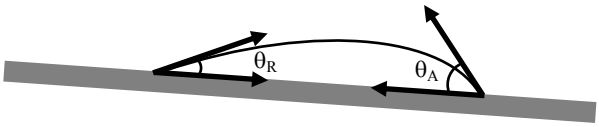

Figure 2.2: Advancing and receding contact angle (θ_A: Advancing contact angle, θ_R: Receding contact angle)

2.1.3. *Objective*

The objective of the work described in this chapter was to evaluate the effects of dissolution on contact angle. Just as physically retracting a sessile drop reduces its contact angle with a surface, it was speculated that dissolution could cause contact angles to be reduced. Long-term dissolution experiments were conducted over the course of days to weeks, examining the dissolution of sessile drops of two DNAPLs, trichloroethylene (TCE) and tetrachloroethylene (PCE), in water and low concentration surfactant solutions, on glass surfaces. A numerical model was also developed on basis of the experimental data to predict the shapes of dissolving drops, based on solution of the Bashforth-Adams equation.

2.2. BASHFORTH-ADAMS EQUATION AND AXISYMMETRIC DROP SHAPE ANALYSIS

2.2.1. *Bashforth-Adams Equation*

The Bashforth-Adams equation is a special case of the Young-Laplace equation of capillarity. The Bashforth-Adams equation can describe the shape of an axisymmetric interface between two fluids as a function of the interfacial tension between the fluids and the density difference between the fluids (4). The equation can be used to predict the shape of a sessile or pendant drop or bubble given the interfacial tension and density

difference with the surrounding fluid and, in the case of sessile drops, the contact angle with the solid surface. The equation is also the basis for measuring surface and interfacial tension based on image analysis of drop shapes (13, 33, 34, 35). The Bashforth-Adams equation is given in equation 2.1 below (4, 5):

$$\frac{1}{R_1/b} + \frac{\sin\phi}{x/b} = 2 + \beta\frac{z}{b} \tag{2.1}$$

where, b is the radius of curvature at the apex of the drop,

ϕ is the angle between the horizontal plane and the tangent to the drop at any point (x, z) on the drop profile, and

R_1 is the radius of curvature of the profile of the drop (i.e., in the plane of the page for a side view of the drop) at the same (x, z) point along the profile.

The parameter β is known as the Bond number or the shape factor and is a ratio of interfacial forces to gravitational forces. The Bond number is given by equation 2.2:

$$\beta = \frac{\Delta\rho g b^2}{\gamma} \tag{2.2}$$

The Bond number encapsulates the effects of interfacial tension (γ) and density difference (Δρ) on the shape of a drop. A positive β produces a sessile drop shape while a negative β produces a pendant drop shape. When β is equals to zero, Δρ equals to zero, in other words no force is acting on the drop and the drop takes a spherical shape. Figure 2.3 shows the dimensionless profile of a Bashforth-Adams drop with all important variables. Note that, a change in interfacial tension (γ), as for example reducing γ will elongate a pendant drop or flatten a sessile drop, but cannot change the sign of β;

conversion of a drop from a sessile shape to a pendant shape can only be accomplished with a density change.

Solution of the Bashforth-Adams equation is achieved by simultaneous solution of equations 2.1 and 2.2 with three additional relationships that can be determined from geometry, equations 2.3-2.5 (33):

$$\frac{1}{R_1} = \frac{d\phi}{ds} \tag{2.3}$$

$$\frac{dx}{ds} = \cos\phi \tag{2.4}$$

$$\frac{dz}{ds} = \sin\phi \tag{2.5}$$

where s is the distance along the profile of the drop from the apex.

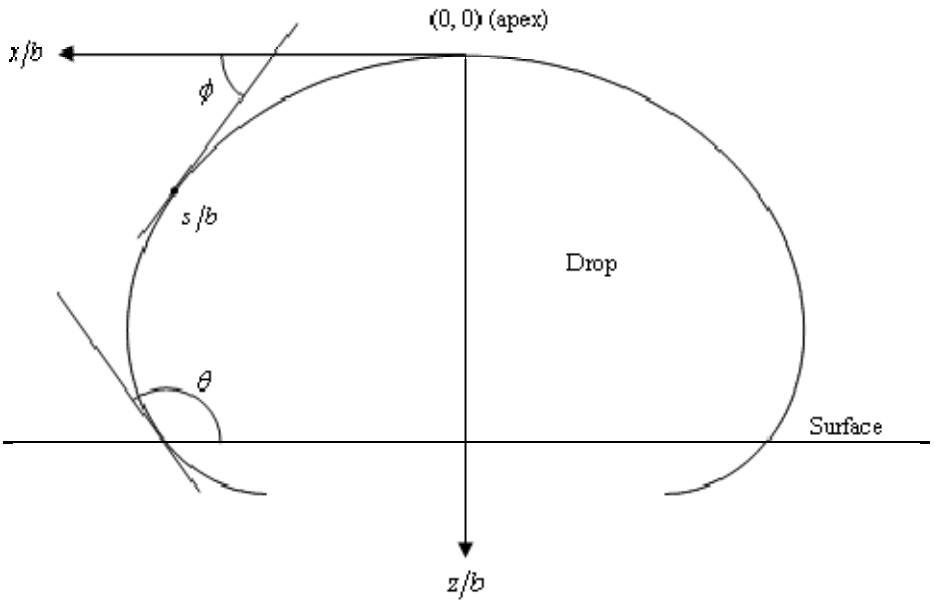

Figure 2.3: Bashforth-Adams dimensionless drop profile corresponding to $\beta = 1.743$. Because the drop is axisymmetric, solution of the Bashforth-Adams equation gives a half profile (i.e.,x positive); in this figure, both sides of the profile have been shown for clarity. In the figure, $\Delta\rho=\rho_{drop}-\rho_{surroundingliquid}$. To solve for a drop with its apex at the bottom, the orientation of the axes and the sign of $\Delta\rho$ are switched.

Solution methods start at the apex of the drop (x=0, z=0, s=0, ϕ=0, $d\phi/ds$=1) and integrate along s to calculate the profile of the drop until a desired ϕ is reached. A number of different methods have been used and higher order Runge-Kutta methods have been shown to be a good choice (13).

Solution of equations 2.1-2.5 gives a dimensionless drop profile (x/b vs z/b); conversion to an actual drop profile requires a reference length to determine b. In the case of a sessile drop, the contact angle (θ) is also needed to define the actual drop profile, because the theoretical profile is truncated by its contact with the surface (Figure 2.3). When contact angle is defined through the drop, the contact angle is equal to the value of ϕ at the intersection between the profile and the surface.

For the work described here, the Bashforth-Adams equation has been used in two contexts: first, a model is used to describe the effect of dissolution on contact angle for a drop for which the footprint is pinned to the surface; second, all drop analyses in this research work were conducted via axisymmetric drop shape analysis of images of drop profiles.

2.2.2. *Axisymmetric Drop Shape Analysis*

Contact angle, drop volume, and interfacial tension were measured using axisymmetric drop shape analysis **(**13, 33, 34, 35**)**. Edge detection made use of the Sobel edge operator **(**33**)**, and drop profiles were fit using a fourth order Runge-Kutta solution of the Bashforth-Adams equation **(**4**)** and nonlinear regression fits based on the Nelder-Mead downhill-simplex algorithm **(**36**)**. Automated software written for this purpose was used to analyze batches of hundreds of images.

2.3. MATERIALS AND METHODS

2.3.1. *Materials*

Tetrachloroethylene (PCE) and Trichloroethylene (TCE) were the DNAPLs selected for this research work. PCE and TCE were selected as they are widely used chlorinated solvents, and are common contaminants at National Priority List (NPL) sites (21, 22). PCE was purchased from Aldrich Chemical Company, Inc. (Milwaukee, WI). TCE was purchased from Fisher Chemical (Fair Lawn, NJ). All DNAPLs had stated purities greater than 99.5% and were used as received. Properties of DNAPLs used in this research work are given in Table 2.1.

TABLE 2.1. Properties of DNAPLs Used in Dissolution Experiments[38]

DNAPL	Formula	Molecular weight (g/mol)	Aqueous Solubility (M)	Density, ρ (g/mL)	Interfacial tension with water γ_{ow} (mN/m)
TCE	C_2HCl_3	131.39	8.37×10^{-3}	1.4642	34.5
PCE	C_2Cl_4	165.83	8.99×10^{-4}	1.6227	47.5

Experiments involving surfactants were conducted with one of the following: cetyltrimethylammonium bromide (CTAB) (a cationic surfactant), sodium dodecylbenzenesulfonate (SDBS) (an anionic surfactant), or Tergitol NP9 (an ethoxylated nonionic surfactant). CTAB and SDBS were purchased from Sigma-Aldrich Co. (St. Louis, MO), while NP9 was provided by Dow Chemical Co. (Midland, MI). CTAB had a minimum stated purity of 99%. SDBS was technical grade surfactant containing approximately 80% dodecylbenzenesulfonate based on total alkylsulfonate content (monodisperse SDBS is not commercially available). NP9 is a commercial ethoxylated surfactant with greater than 99% active content. For SDBS and NP9, molar concentrations are based on average molecular weights (348.48 and 616.82 g/mol, respectively). All experiments were conducted at concentrations below surfactant critical micelle concentrations (CMCs). Although surfactant-based remediation applications typically involve concentrations much higher than the CMC (e.g., (29, 40)), the purpose of this work was to examine the possible effects of low concentration surfactants either present initially in the subsurface (e.g., through incomplete wastewater treatment), or entering the environment with the DNAPL. The CMCs of CTAB and SDBS have been reported to be 9.2×10^{-4} M (2) and 1.7×10^{-3} M (41) in the absence of added salt, respectively. The CMC of NP9 is estimated to be 9.4×10^{-4} M (42). All surfactants were used as received.

All experiments reported in this chapter were conducted on silicate glass surfaces (24 mm x 40 mm Gold Seal cover glass (Erie Scientific, Portsmouth, NH)). Glass surfaces were selected to represent the surfaces of sandy, low-carbon aquifer materials. Preliminary experiments on mica surfaces found results quantitatively similar to those of

experiments on glass slides, so work with mica was not pursued further. Glass slides and other glassware were cleaned prior to use by rinsing in HPLC-grade methanol (Sigma-Aldrich), soaking for 24 h in 1% LIQUI-NOX solution (Alconox, Inc., White Plains, NY) followed by at least 10 rinses in Nanopure water (Barnstead, Dubuque, IA). Cover glass surfaces were not reused. All solutions were prepared using Nanopure water.

2.3.2. *Experimental Procedures: Dissolution Experiments*

Dissolution of DNAPL sessile drop in aqueous solution was observed over a long period of time (days to weeks). Experiments were conducted in rectangular optical cells, open to the atmosphere (Figure 2.4). Two different optical cells were used: one 5 cm x 5 cm x 5 cm optical glass cell (purchased from Fisher Scientific) and one 4.5 cm x 4.5 cm x 3 cm quartz cell (purchased from Rame´-Hart (Mountain Lakes, NJ)). No differences were observed or expected between the cells, with the exception of slightly different dissolution rates because of the different volumes and air/water interfacial areas in the cells. Because the purpose was not to examine dissolution rates, no attempt was made to prevent escape of TCE or PCE to the vapor phase. Several experiments (data not shown) were conducted using nitrogen sparging to accelerate dissolution, but the approach was abandoned because of difficulty preventing the nitrogen bubbles from disrupting the drop, and because of foaming in the surfactant solutions.

To conduct a dissolution experiment, an optical cell was initially filled with aqueous solution and glass slides were positioned on a stainless steel or aluminum stage within the cell. A sessile drop was then formed manually in the center of the glass slide using a syringe with a 30 gauge needle (Figure 2.4). Drops were generally formed at or

near their advancing contact angle. Drop volumes used in this work ranged from a few micro-liters to approximately 100 μL.

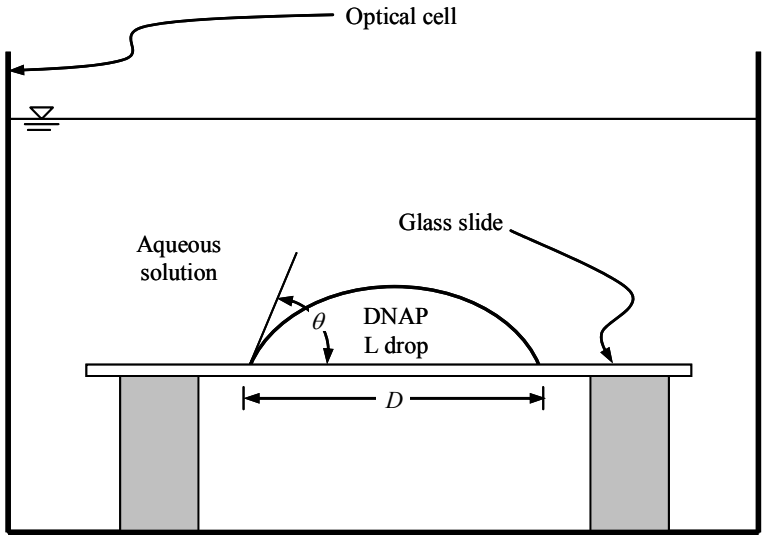

Figure 2.4: Schematic diagram of the optical cell. View of DNAPL sessile drop dissolution from the camera direction. (D: contact diameter)

Following placement of the drop, the camera was focused, and a reference dimension was taken by submerging a vertical pre-calibrated cylindrical reference directly above the drop. The reference was then removed, and imaging was started, typically within a few minutes of the time the drop was formed.

Experiments were conducted in two parallel experimental setups, each like the one shown in Figure 2.5. Each setup consists of one 30W halogen lamp, one ground-glass diffuser, an optical cell containing the solution, the glass surface and the DNAPL drop, and a CCD camera. All components except the cameras are height adjustable. The platform on which both setups are constructed can be leveled by adjustment of six height-adjustable feet.

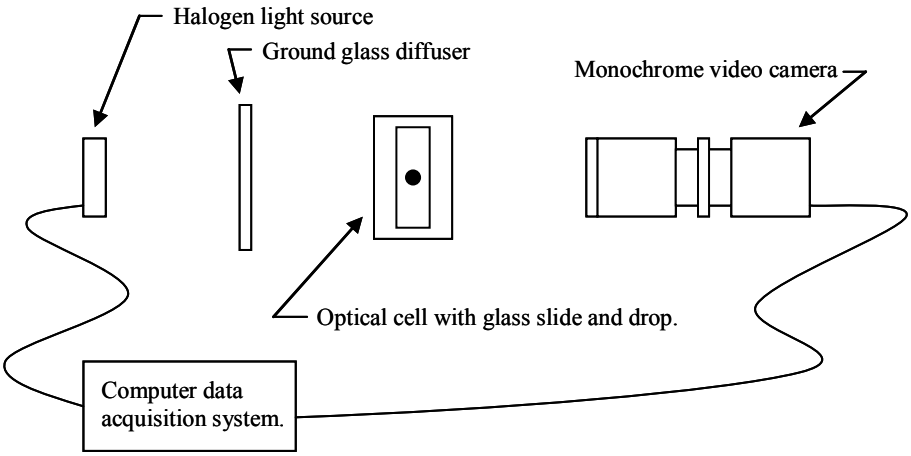

Figure 2.5: Schematic diagram of the experimental setup (Top view)

Each camera is mounted on a Bogen-Manfrotto (Ramsey, NJ) model 410 geared head, allowing fine angle adjustments to be made. Cameras used were: one Hitachi (Woodbury, NY) KP-M2 camera, and one Pulnix (Sunnyvale, CA) TM-7CN camera. Both cameras are 525 line, 1/2 inch CCD monochrome cameras. Both cameras were equipped with Computar TEC-55 telecentric lenses with 2x extenders (Computar Optics, Inc., Hudson, NH). Green filters were used to improve image sharpness. Imaging was computer-controlled using software written for the purpose. To prevent heating of samples over the long duration of experiments, halogen lights were controlled by computer-controlled relays, which illuminated them only when images were taken. Images were taken at time intervals ranging from a few seconds at the start of each experiment, to 30 min after approximately 1 day. More rapid imaging at the start was intended to capture initial rearrangement of the drop as the interfacial region of the water and DNAPL became mutually saturated and (where appropriate) surfactant adsorbed at interfaces. Although temperature was not controlled in experiments, the laboratory

where experiments were conducted typically maintains a temperature ranging from approximately 20 to 22 °C.

2.3.3. *Experimental Procedures: Receding Contact Angle Measurement*

The receding contact angle of TCE in water was determined using a J-shaped needle, with its tip inserted upward through a drilled hole in a glass slide. A TCE drop was formed and then taken through a sinusoidal volume range (approximately 30-220 μL, at a rate of 1 μL/s) using an I.T. Concept Tracker system (Theta Dyne Corp., Charlottesville, NC). Contact angles were taken as the value of the Bashforth-Adams ϕ corresponding to the intersection of the theoretical profile and the surface. Similar analyses conducted manually produced very similar results, to within a few degrees.

2.3.4. *Dissolution Model*

As a part of the work described below, a model was developed to predict the shapes of dissolving drops for which their contact diameter remains constant, based on solution of the Bashforth-Adams equation. The model requires specification of a contact diameter (D), interfacial tension (γ), and density difference ($\Delta\rho$), and then calculates the volume of a theoretical drop for a range of contact angles, from 1° up to a specified maximum. The solution for the model is the same as for the drop shape analysis as described above, but the specified drop diameter is used as reference length. For each contact angle, θ, the solution is iterated by setting:

$$b^i = \left\{ D \Big/ \left(\frac{x}{b} \right)^i_{\phi=\theta} \right\} \tag{2.6}$$

Calculating β from equation 2.2, and then solving the Bashforth-Adams equation at $\phi=\theta$ to determine $(x/b)_{\phi=\theta}^{i+1}$), which is used in equation 2.6 to determine b^{i+1}. Iteration continues until the value of β converges for the current θ value, and then θ is increased and the procedure is repeated.

2.4. RESULTS AND DISCUSSION

In course of dissolution, it was observed that dissolving drops tend to retain their initial contact diameters during dissolution for a wide range of systems; i.e., the original footprint of the drop on the surface does not change during dissolution.

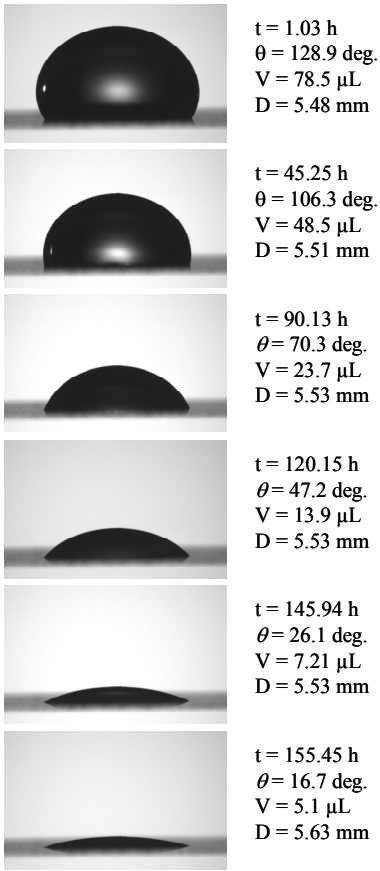

Figure 2.6: Dissolution of TCE on glass in Nanopure water over approximately 6.5 days (155 h). Time (t), contact angle (θ), drop volume (V), and contact diameter (D) are indicated. *(Data from Mohammad and Kibbey, 2005 (43))*

This is illustrated in Figure 2.6, which shows images of a drop of TCE dissolving in Nanopure water over approximately 6.5 days. It is apparent from Figure 2.6 that although drop volume decreased by about 93.5% (from 78.5 μL to 5.1 μL) in approximately 6.5 days, the contact diameter remains constant. Although a small difference in contact diameter is reported (from 5.48 mm to 5.63mm in approximately 6.5 days), the difference is more as a result of difficulty to fit a very flat sessile drop (nearly dissolved) and thus locate the base of the drop with sub-pixel accuracy. Despite the slight variations in measured values, it is apparent from Figure 2.6 that the contact diameter of the dissolving TCE drop remains essentially constant. Note that, although this result has been observed for different DNAPLs in a range of solutions, preliminary experiments examining volatilization of liquids in air (data not shown) did not observe constant contact diameters, although contact angles were still observed to decrease during volatilization.

Figure 2.7 represents quantitative analysis of the experimental data corresponding to the images shown in Figure 2.6. Figure 2.7A shows the contact angle (measured through the drop) of TCE drops as a function of drop volume in course of dissolution over approximately 6.5 days. The vertical arrows indicate the contact angle and volume of TCE drops shown in Figure 2.6. The dashed line indicates the receding contact angle measured in a separate experiment as described in section 2.3.3. So dissolution causes contact angle of TCE to drop well below receding contact angle. One possible reason may be the difference of rate of volume change between dissolution and receding contact angle measurement (rate of volume retraction in course of receding contact angle measurement).

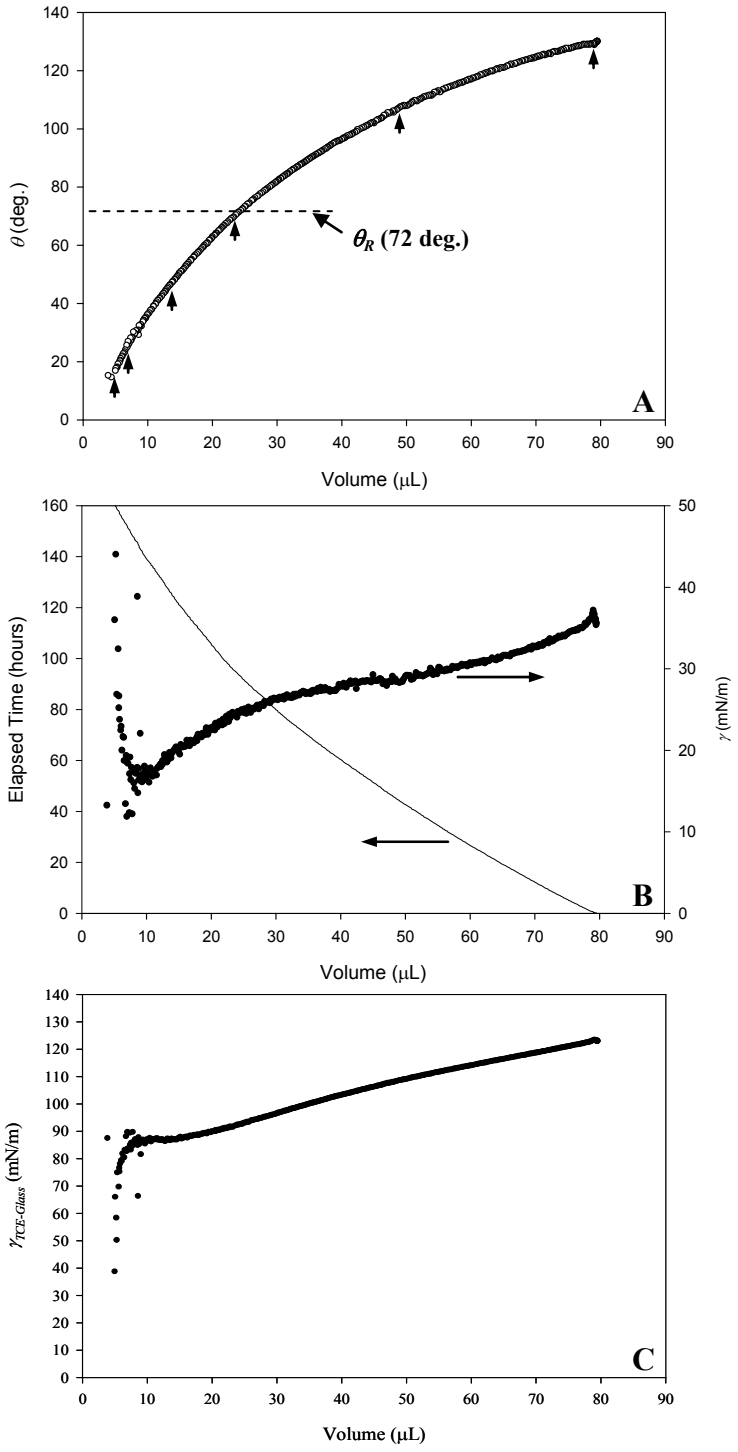

Figure 2.7: Dissolution of TCE on glass in Nanopure water over approximately 6.5 days (155 hr). (A) Contact angle versus drop volume. Vertical arrows indicate images in Figure 2.6. Dashed line indicates measured receding contact angle, θ_R. (B) Interfacial tension and elapsed time versus volume. *(Data from Mohammad and Kibbey, 2005 (43))* (C) TCE-Glass Interfacial Energy, $\gamma_{(TCE\text{-}Glass)}$ versus volume.

The rate of drop retraction in receding contact angle measurement was 1μL/sec (section 2.3.3) where as the rate of volume change due to dissolution of TCE drop was on an average 0.5 μL/hr (from 78.5 μL to 5.1 μL in approximately 155.5 hours). Measured receding angles were not found to be rate dependent. In other words, a faster volume retraction rate or even a manual volume retraction also produces similar result. Although the faster volume retraction rate (compare to dissolution) may impart enough energy to overcome the pinning of drop footprints and lead to a higher receding angle value.

At the end of the dissolution data shown in Figure 2.7A (to the left of the leftmost data point shown in Figure 2.7A), at volume of approximately 5 μL and a contact angle of approximately 15°, the contact diameter of the drop slipped to approximately 3.3 mm. As a result the contact angle increased and the drop became asymmetric, hence no further analysis was possible. Further imaging of the dissolution of asymmetric drop showed that the contact angle decreased all the way to 0° as the drop was completely dissolved. So, for this system, receding contact angle does not have any practical impact as the drop gets completely dissolved. This result was consistent for all the dissolution experiments where the drop was allowed to dissolve completely.

Figure 2.7B shows both the interfacial tension of the drop during dissolution and the time each image was collected as a function of drop volume. The interfacial tension shows an initial increase and then shows a gradual decrease with the decrease of drop volume in course of dissolution. The initial increase of interfacial tension may be because of the mutual saturation of interfacial regions of the two phases (Water/TCE). After 3 hours of equilibration period, the interfacial tension of TCE was 34.8 mN/m, which is consistent with the reported value **(**38**).** But after 1 day of dissolution, the

interfacial tension of TCE drops to 30.8 mN/m and continually drops through out the experiment. This behavior of interfacial tension dropping has been observed in all different systems studied in dissolution experiments. This interfacial tension drop may results from one of three possible factors:

(i) Drop asymmetry: Increasing drop asymmetry in course of dissolution may result in erroneous measured interfacial tension as the Bashforth-Adams equation assumes asymmetric drop. Although the drop images from these dissolution experiments appear to be highly symmetric, top views were not imaged. So any three-dimensional asymmetry has not been observed. Preliminary experiments applying Bashforth-Adams equation to intentionally asymmetric drops predicted lower interfacial tension even though a very good fit to profile was achieved. More work is needed to determine if the magnitude of error is sufficient to explain the observed decrease in interfacial tension.

(ii) Trace impurity of DNAPLs: Long term dissolution may cause aging of interface and trace impurities of DNAPLs may adsorb gradually on the interface. Although DNAPLs of high purity (more than 99.5% pure) were used in the experiments, a trace amount of slowly adsorbing impurities may cause the interfacial tension reduction. Impurities from other sources (the atmosphere, water) were eliminated by a series of controlled experiments (sealed optical cell, different water sources) which exhibit same results as shown in Figure 2.7B.

(iii) Line tension effect (44, 45, 46**):** As contact diameter remains constant, it may overconstrain the solution of Bashforth-Adams equation. That means when drop decrease in volume the tension along the contact diameter (line tension) may have greater

impact and leads to produce erroneous solution. However, decrease in interfacial tension was observed even for drops too large to be influenced by line tension (44, 45, 46) suggests that line tension unlikely be the key factor.

Experiments, where an existing aged drop (partially dissolved and exhibiting a low interfacial tension) was collected with a syringe, and then used to form a new drop in the same solution found that the new drop had an interfacial tension similar to the initial interfacial tension of the original drop, and then the interfacial tension decreased over time at a rate similar to the interfacial tension decrease of the original drop. This result could also be consistent with all the three possibilities explained above as the formation new drop would eliminate the drop asymmetry due to dissolution, would create a new interface and would release any stresses at the drop interface.

In Figure 2.7B, interfacial tension values are considerably scattered below volume approximately 10 μL. One possible reason is drop shape. At volume less than 10 μL, the drops became too flat to achieve a good fit while doing drop profile analysis (13). Another possible reason is surface area to volume ratio of the drop, which increases with the decrease of drop volume. As a result, the influence of gravity on the drop decreases. In other words, for a small drop, a large variation of interfacial tension produces a small amount of change in the drop shape. Hence it becomes difficult to measure interfacial tension accurately from drop shape analysis. Considering this, for all analyses in subsequent figures where interfacial tensions are presented, interfacial tension data was shown only down to a volume of 10 μL.

Figure 2.7C shows the TCE-Glass interfacial energy ($\gamma_{TCE\text{-}Glass}$) in the course of dissolution for the TCE drop as a function of drop volume. $\gamma_{TCE\text{-}Glass}$ gradually decreases over time as TCE drop dissolved in Nanopure water. $\gamma_{TCE\text{-}Glass}$ was calculated using Young's equation (equation 1.1), where $\gamma_{Nanopure\ water\text{-}Glass}$ was considered as 100 nN/m (50). Note that this calculation suggests that the decrease in contact angle may be due to the decreasing TCE-Glass interfacial energy, which itself may be the result of adsorption of impurities at the solid surface. However it is not clear that Young's equation is valid in this context. Furthermore, new drops formed on a surface after complete dissolution of a drop showed similar initial contact angle to the original drop, suggesting solid surface adsorption is not contributing to the observed behavior.

Considering these experimental results, a numerical model was developed to model the effect of dissolution on contact angle if contact diameter is held constant (i.e., the footprint of the drop is pinned to the surface). The model is based on solution of Bashforth-Adams equation, which describes the shape of an axisymmetric drop of a particular interfacial tension and density difference from the surrounding fluid. Details of the numerical model and its solution are given in the Section 2.3.4.

The model can then be used to generate the predicted drop profile over time for a dissolving drop with a fixed contact diameter, as well as the predicted contact angle as a function of volume during dissolution. Figure 2.8 shows model predictions for two drops with the density of TCE in water, for a range of interfacial tensions. Figure 2.8A corresponds to dissolution of a drop with a 2 mm contact diameter (a small drop), while Figure 2.8B corresponds to dissolution of a drop with a 10mm contact diameter (a large

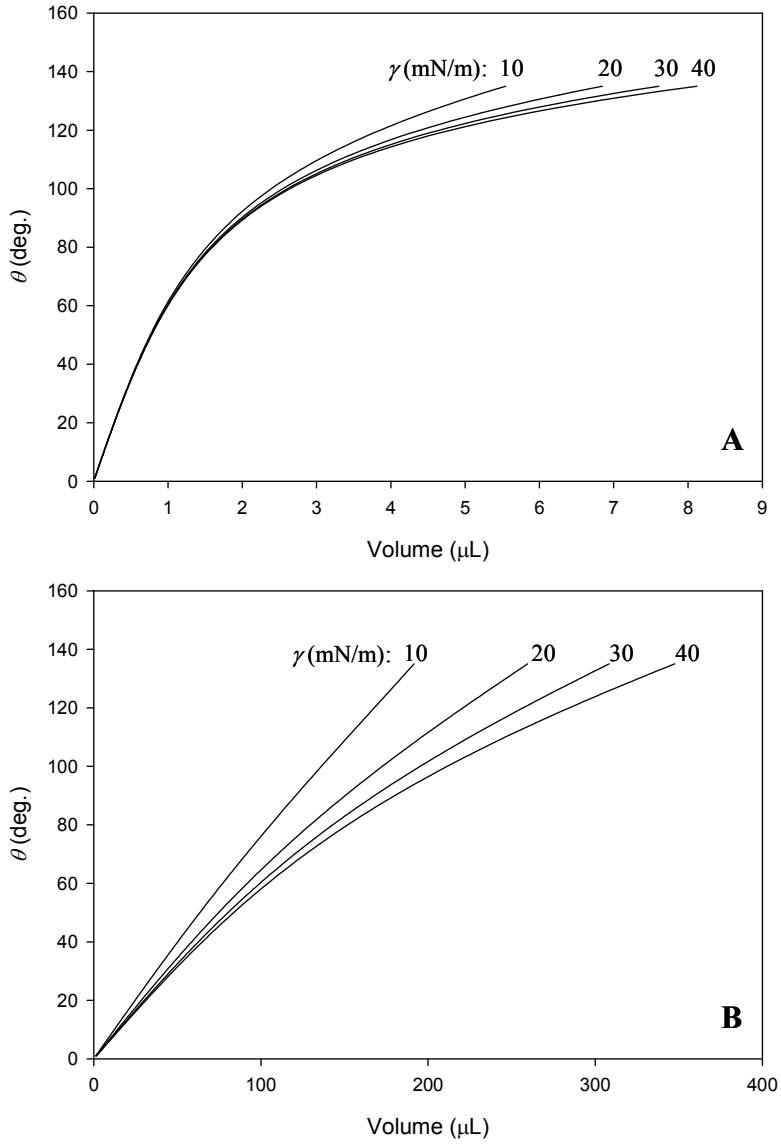

Figure 2.8: Model-predicted contact angle (θ) versus volume for drops of a fluid with the density of TCE in water, shown for a range of interfacial tensions (γ). (A) Small drop, with D=2 mm. (B) Large drop, with D=10 mm. *(Data from Mohammad and Kibbey, 2005 (43))*

drop). In both cases, the initial contact angle was 130^0. As the contact diameter is fixed, the volume of each drop for a particular contact angle varies with interfacial tension. In other words, smaller interfacial tension will correspond to a flatter drop. Again for a

particular volume of drop, smaller interfacial tension will correspond to a smaller contact angle.

From Figure 2.8A and B, it is apparent that, for a particular liquid, the change of contact angle of a large drop with dissolution is a strong function of interfacial tension, with lower interfacial tensions producing a near linear relationship between contact angle and volume. Smaller drops, or larger drops with higher interfacial tensions, show a nonlinear relationship between contact angle and volume, with large initial changes in volume having little effect on contact angle, but small changes in volume having a much greater effect on contact angle as the drop becomes smaller. In all cases dissolution causes contact angle to decrease.

Figure 2.9 shows the application of the dissolution model to the dissolution of sessile drops of TCE in three different solutions. Figure 2.9A shows dissolution of TCE in water (data from Figure 2.6) over 6.5 days, Figure 2.9B shows dissolution of TCE in 8.4×10^{-5} M NP9 over 7.2 days, and Figure 2.9C shows dissolution of TCE in 2.2×10^{-4} M SDBS over 6.0 days. Firm lines indicate model prediction; each line corresponds to dissolution of a specific drop at certain interfacial tension. In Figure 2.9, dissolution of TCE in all three systems (water, NP9 and SDBS) shows a rapid interfacial tension drop at the beginning of the experiment. Then the interfacial tension gradually decreased in course of dissolution. This rapid interfacial tension reduction is due to the mutual equilibration of the drop at the interface region with the surrounding liquid. Initial rapid interfacial tension drop was also accompanied by increase in contact angle and contact diameter. In Figure 2.9A, this effect is less evident as the imaging started 25 minutes after the dissolution experiment started. Equilibration period was about 1 to 1.5 hours in

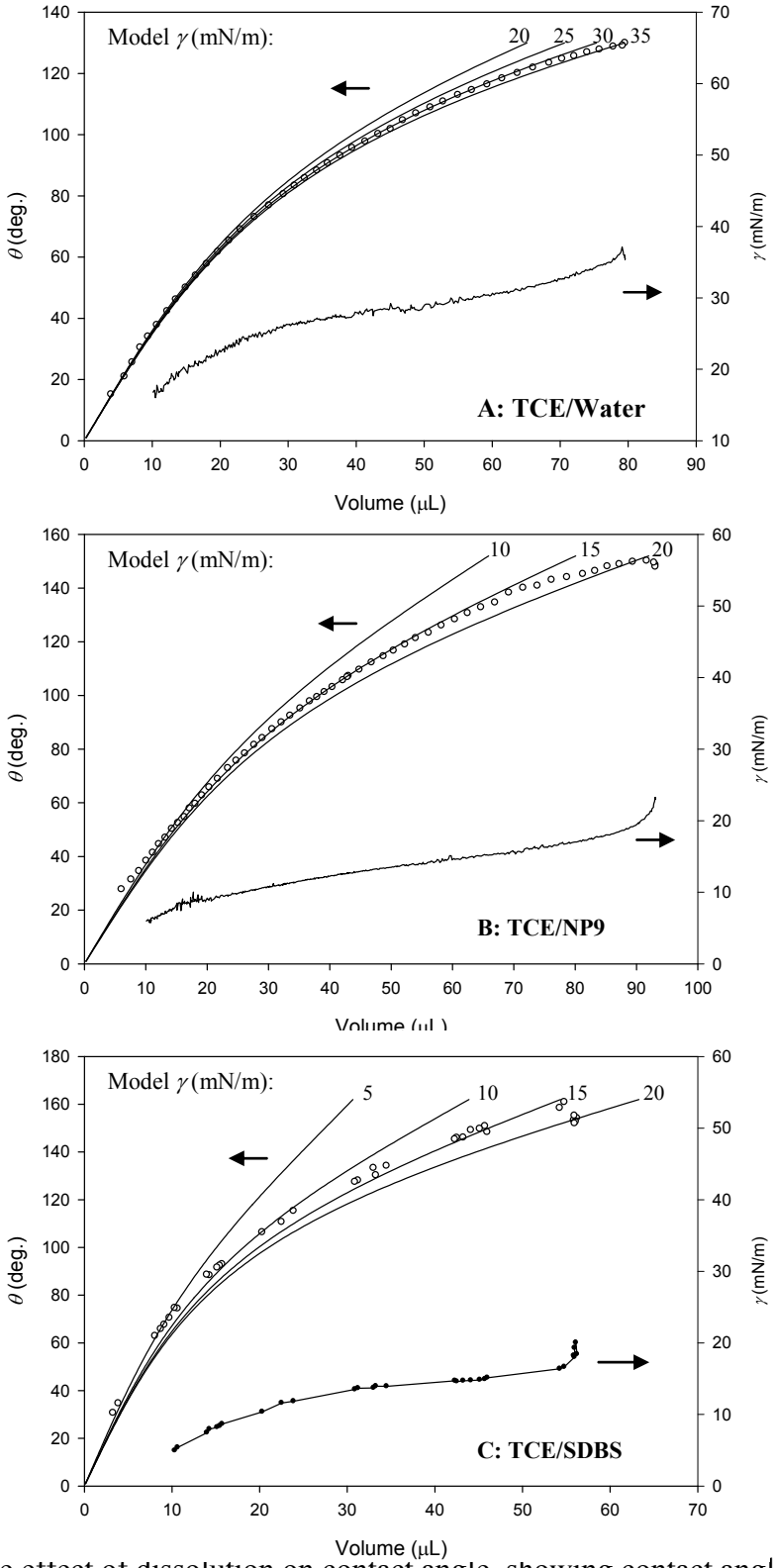

Figure 2.9: The effect of dissolution on contact angle, showing contact angle (θ) and measured interfacial tension (γ) as a function of volume. Model predictions corresponding to the indicated interfacial tension (γ) values are shown. (A) TCE in Nanopure water. (B) TCE in 8.4×10^{-5} M NP9 solution. (C) TCE in 2.2×10^{-4} M SDBS solution. *(Data from Mohammad and Kibbey, 2005 (43))*

all the systems. For modeling purpose, initial contact diameter and contact angle was taken after the equilibration period.

From Figure 2.9, it is apparent that the model does predict the contact angle/volume dissolution behavior for all three systems pretty well, including the effects of changing interfacial tension. The contact angle data initially lays on the higher interfacial tension line (of the model prediction) and gradually follows the lower interfacial tension line as dissolution progressed. And the interfacial tension data agrees with the model prediction as well.

Figure 2.10 shows the effect of dissolution on contact angle for two small drops of PCE, one in water and one in 1.2×10^{-4}M CTAB solution. Again firm lines indicate model prediction of the dissolution of PCE. It is apparent from the figure that the CTAB solution had adsorbed substantially to the glass surface prior to the introduction of PCE, causing the PCE to be the wetting phase. In both cases, the model provides a very good prediction of the effects of dissolution on contact angle.

Although drops of PCE do remain pinned during dissolution, and as such follow model-predicted trends, more work is needed examining the dissolution of larger PCE drops. Because for small drops, model predicted curves of contact angle versus volume are very insensitive to interfacial tension (Figure 2.8). The solubility of PCE is much lower (approximately an order of magnitude lower) than that of TCE. So the aqueous solution becomes saturated after a much smaller volume has dissolved. Future work should use a flow-through system to use larger (volume) PCE drop for the dissolution experiments.

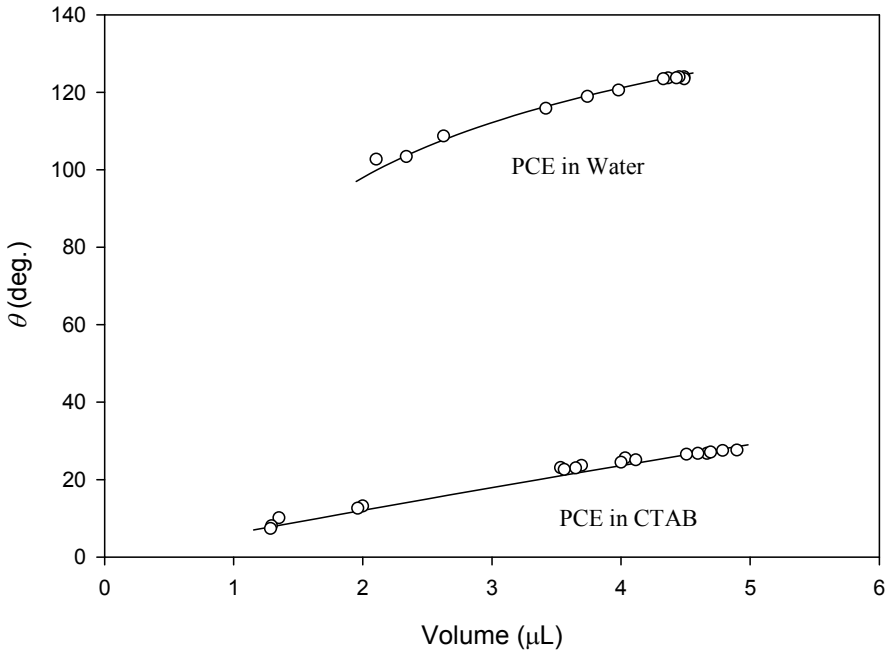

Figure 2.10: Dissolution of PCE in Nanopure water and 1.2 x 10^{-4} M CTAB solution. Model predictions are shown, based on the reported interfacial tension of pure PCE (47.48 mN/m). The small size of drops precludes accurate interfacial tension measurements. *(Data from Mohammad and Kibbey, 2005 (43))*

While contact angle of DNAPLs were gradually decreasing and contact diameters were pinned in course of dissolution in most of the systems, there were some occasional slip (of contact angle and contact diameter) observed in some dissolution experiments. Figure 2.11 shows the dissolution of TCE in Nanopure water, where some random slips were observed. Figure 2.11A represents the change of contact angle and interfacial tension of TCE as a function of volume in course of dissolution in water. Firm lines indicate model prediction of the dissolution of TCE. Figure 2.11B represents contact diameter of dissolving TCE in water as a function of volume.

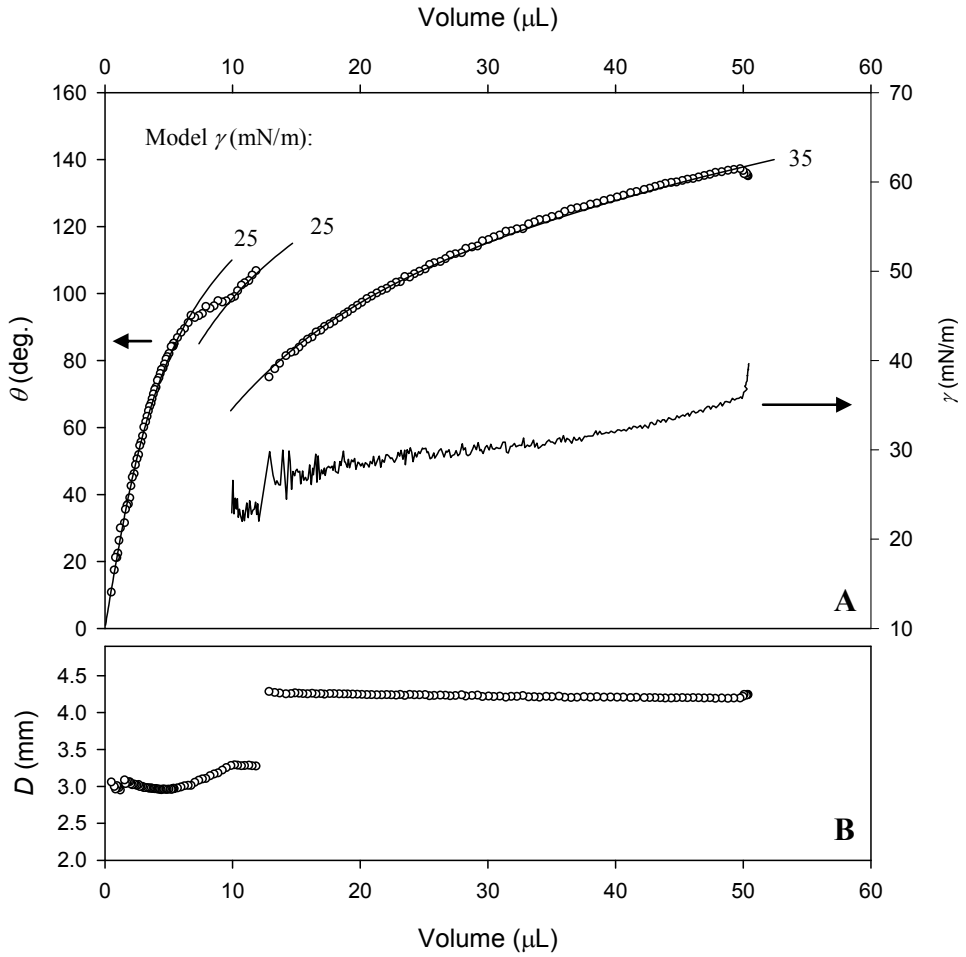

Figure 2.11: Dissolution of TCE in Nanopure water, showing the effects of slip/stick behavior. Model predictions are shown for segments where drop contact diameter remains constant. *(Data from Mohammad and Kibbey, 2005 (43))*

Like other experimental data, a rapid decrease in interfacial tension with corresponding increase in contact angle took place at the beginning of the experiment. Then the contact angle gradually decreased till the volume reached approximately 13 μL. The contact diameter slipped at one side of the drop while the other side remained pinned and the contact angle jumped from 74.8° to 107.8° (Figure 2.11). The drop remained pinned down to a volume of approximately 9 μL (13 hour later), began to slip again, and then eventually was pinned again to a volume of approximately 4 μL (approximately 40

hour after the initial slip). After again slipped at this volume, the drop remained pinned till completely dissolved.

Kwok et al. (37) observed similar slip and stick behavior while studying expansion of liquid drops on a non polar surface in air. He studied 30 different liquids and found this slip/stick behavior in 21 liquids. While expanding the drops, he observed contact diameter to stick on the non polar surface and contact angle started to increase. At certain point the drop slipped (contact diameter expanded to a new diameter) and the contact angle decreased in course of drop expansion. The authors attributed the behavior to the asymmetry of the drops.

2.5. CONCLUSION

DNAPL drops are highly unlikely to be positioned on flat surface (as examined in this work) in the subsurface aquifer system. More likely DNAPLs are to be entrapped in the aquifer pores and initially behave as non wetting phase. In course of dissolution, if contact angle between DNAPL and aquifer surface reduces (as observed in this work), DNAPL will gradually change into wetting phase. If the contact angle approaches to zero, then additional hydrostatic force will be needed to mobilize the DNAPLs. This scenario may lead to flow bypassing the smaller pores and cause longer remediation time.

Future experiments examining dissolution from capillaries, and the effects on corresponding forces needed to cause them to drain would provide useful insight into this possible scenario. Additional experiments examining the effects of high concentration surfactants likely to be used in remediation applications would also be useful. One preliminary experiment has conducted with TCE in a high concentration SDBS solution

(data not shown) showed some slipping in the drop footprint with dissolution, but nevertheless found a continuous decrease in contact angle with dissolution. More work would be needed to understand this behavior and to determine the surfactants and conditions likely to produce it.

CHAPTER 3

DYNAMICS OF MIXING AND INTERFACIAL ADSORPTION DURING DROP EXPANSION

3.1. INTRODUCTION

Equilibration of surfactant solutions at surfaces and interfaces is an important phenomenon in many practical applications ranging from subsurface remediation, detergency, coating processes, enhanced oil recovery and emulsification to personal care products. When surfactant adsorbs on a surface or interface, the surface/interfacial tension is not initially equal to the equilibrium surface/interfacial tension of the system. Depending on the fluid types, phase volumes, surfactant type, surfactant concentration and interfacial area it may take milliseconds to days to attain equilibrium surface/interfacial tension. So for different practical applications, it is very important to understand the adsorption kinetics of surfactant and the corresponding effect on dynamic surface/interfacial tension over time. The objective of this work is to examine the dynamics of surface/interface equilibration of surfactant solution in the course of dilution. The adsorption of three different surfactants, cetylpyridinium cloride (CPC), sodium octylbenzenesulfonate (SOBS), and polydisperse commercial nonylphenol ethoxylate, Tergitol NP15, onto the air-water interface has been studied by pumping Nanopure water into surfactant pendant drops at a constant flow rate to cause dilution. Surface tension in the course of dilution was measured and compared with the equilibrium surface tension. A simple, quantitative dilution model based on diffusion/mixing has been developed to

understand the dynamics of mixing and interfacial adsorption of surfactant onto the air-water interface.

3.1.1. *Surfactant*

Surfactant (surface active agent) has the property to adsorb onto the surface or interface of the system. Surfactant adsorption at surfaces/interfaces is an important phenomenon in many different practical applications ranging from subsurface remediation, detergency, coating processes, enhanced oil recovery and emulsification to personal care products (1, 2). When surfactant adsorbs onto the surface/interface, the surface/interfacial free energy of the system changes due to the adsorption. The surface/interfacial free energy is the minimum amount of work required to create that surface/interface and surface/interfacial tension is the free energy per unit area of that surface/interface (2, 4, 5). At low concentration, surfactant molecule remains unassociated to each other and known as monomer. Surfactant monomer has a characteristic molecular structure consisting of one or more hydrophilic head groups and one or more hydrophobic tail groups (2) (Figure 3.1). Depending on the environment contributing to the surface/interface, the monomer can adsorb onto the surface/interface by associating its head or tail groups together and can change the amount of energy required to create the surface/interface (surface/interfacial tension) (2, 8).

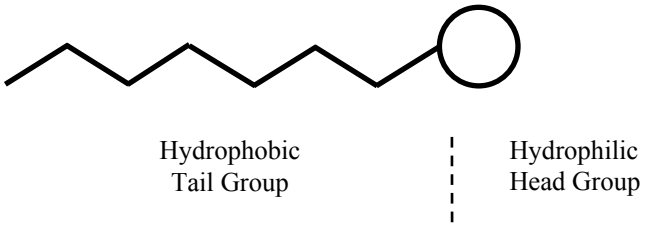

Figure 3.1: Schematic diagram of surfactant monomer.

In aqueous solution, when surfactant concentration increases above a certain concentration known as critical micelle concentration (CMC), the monomers aggregate into a cluster with their hydrophobic groups directed toward the interior of the cluster surrounded by their hydrophilic groups directed toward the exterior (solvent) to minimize free energy of the solution (2). This cluster is known as micelle. So beyond CMC, the available monomer to adsorb on the surface/interface remains constant.

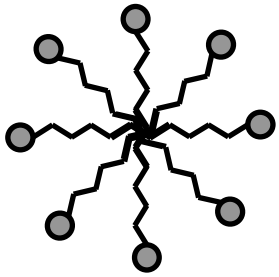

Figure 3.2: Schematic diagram of Micelle

3.1.2. *Surface Tension Curve*

Surfactant monomer absorbs on the surface and generally reduces the surface tension of the system. Below the CMC, as concentration of surfactant increases, more monomers adsorb on the surface and decrease surface tension of the system. Beyond the CMC, available unassociated monomer concentration for adsorption remains constant and the surface/interfacial tension also becomes constant. Figure 3.3 shows a surface tension curve (surface tension variation over concentration) of a surfactant, cetylpyridinium chloride (CPC). Below the CMC, the surface tension of CPC decreases as CPC concentration increases. Above the CMC, the surface tension becomes constant.

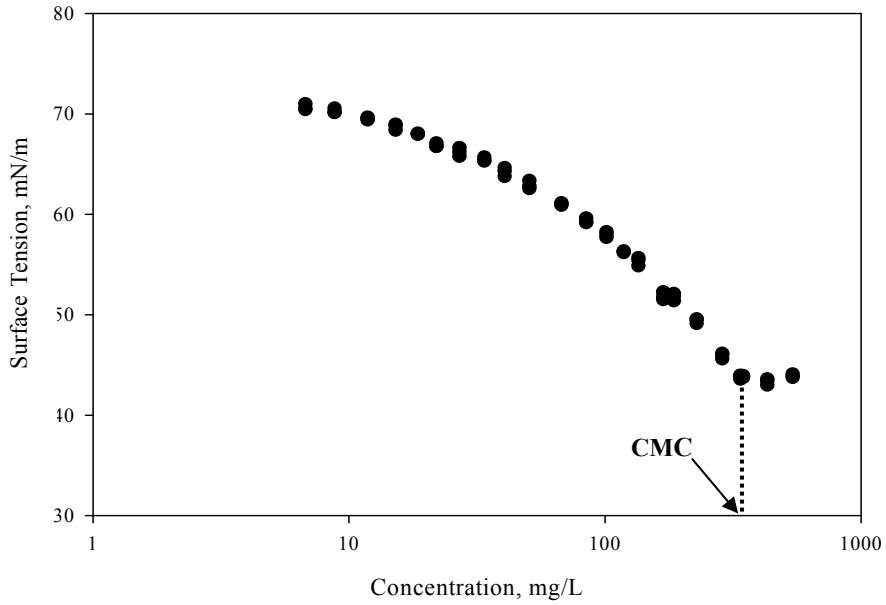

Figure 3.3: Equilibrium surface tension of cetylpyridinium chloride (CPC) as a function of concentration.

3.1.3. *Surfactant Adsorption and Dynamic Surface Tension*

When a system consists of two immiscible phases, the boundary between the phases is known as an interface. When one of the phases is gas, the boundary between the phases is known as a surface (2, 3).

When surfactant monomer first adsorbs onto the surface/interface, the surface/interfacial tension, γ, is not equal to the equilibrium surface/interfacial tension, γ_{eq}. Because of the concentration gradient of surfactant monomer between the bulk phase and the surface/interface, surfactant monomer continues to adsorb on the surface/interface. Over time, the concentration of surfactant monomer at surface/interface reaches a dynamic equilibrium (the rate at which monomer arrives at the surface/interface is equal to the rate at which monomer leaves the surface/interface) and

surface/interfacial tension (γ) becomes equal to the equilibrium surface/interfacial tension (γ_{eq}) (6, 7, 8). There are various techniques available for measuring dynamic surface tension including maximum bubble pressure method (9), drop volume method (10), pendant drop method (11, 12, 13).

Direct measurement of the amount of surfactant adsorbed per unit area is avoided because of the difficulty of isolating the interfacial region from the bulk phase (2). Instead, surfactant adsorbed per unit area is calculated indirectly from the surface/interfacial tension measurements. Surface/interfacial tension is plotted as a function of concentration of surfactant (Figure 3.1). From such a surface/interfacial tension curve, surfactant adsorbed per unit area can be calculated by using Gibbs adsorption equation **(3.2)**:

$$d\gamma = \sum_i \Gamma_i d\mu_i \qquad (3.2)$$

Where, d γ = change in surface/interfacial tension

Γ = surface excess concentration per unit area of interface

μ = chemical potential of any component of the system

And $$\mu = -RT \sum_i \Gamma_i d \ln a_i \qquad (3.3)$$

Where, a_i = activity of any component

R = gas constant and

T = absolute temperature

Various adsorption models have been developed to describe dynamic surface/interfacial tension and adsorption phenomena of surfactant. The work by Ward and Tordai is considered to be pioneering in this field of study. In 1946 they first published a mathematical analysis for surfactant adsorption by using a diffusion controlled model (14). Their model accounts for diffusion of surfactant monomers from bulk phases to interfaces, and also diffusion of surfactant monomers from interfaces to bulk phases when the interfaces become saturated (14). Later numerous theoretical and numerical studies were published to improve the model given by Ward and Tordai (e.g., (7, 15, 16)). In 2000, J. Liu and U. Messow showed that Ward and Tordai solution is applicable for only boundary condition, $x>0$. And Liu et. al. solved the diffusion equation for boundary condition $x\geq 0$ (16). In 2004, Chaodong Yang and Yongan Gu solved the diffusion equation by using semidiscrete Galerkin finite element method (7).

In these adsorption studies, either a pendant drop of surfactant was formed in the air by using a syringe (7) or air bubble was formed in surfactant solution (16) and that surfactant drop or air bubble was held to study surfactant adsorption on surface/interface over a period of time.

3.1.4. *Objective*

In the work described here, dynamic surface/interfacial tension of surfactant solution has been studied and compared with the equilibrium surface tension to understand the dynamics of mixing and surface/interfacial adsorption in course of continuous new surface/interface formation by drop expansion. Adsorption vs. mixing plays a key role in surface/interface equilibration process. Diffusion causes mixing of

bulk organic liquid (surfactant) phase to water. It is hypothesized that adsorption of surfactant to the surface/interface is faster than diffusion/mixing. So when a drop of liquid is diluted the concentration at the surface/interface will be higher than the average bulk phase concentration, and that leads to a lower instantaneous surface/interfacial tension compare to the equilibrium surface/interfacial tension. Eventually when the bulk phase of surfactant reaches equilibrium concentration by diffusion/mixing, the surface/interfacial tension becomes equal to the equilibrium surface/interfacial tension.

3.2. MATERIALS AND METHODS

3.2.1. *Materials*

Surfactants used in this study are one cationic surfactant, cetylpyridinium chloride (CPC), one anionic surfactant, sodium octylbenzenesulfonate (SOBS) and one nonionic surfactant, one polydisperse commercial nonylphenol ethoxylate, Tergitol NP15. CPC was purchased from Sigma-Aldrich Co. (St. Louis, MO), SOBS was purchased from Aldrich Chemical Company, Inc. (Milwaukee, WI), and NP15 was donated by DOW (Midland, MI). In the experiments involving SOBS, solution with excess Na^+ ion (sodium chloride, NaCl salt) was used below the CMC to avoid precipitation. NaCl was purchased from Fisher Scientific (Fair Lawn, NJ). All the chemicals had stated purities of 99% or higher. All the glassware were cleaned prior to use by rinsing in HPLC-grade methanol (Sigma-Aldrich), soaking for 24 h in 1% LIQUI-NOX solution (Alconox, Inc., White Plains, NY) followed by at least 10 rinses in Nanopure water (Barnstead, Dubuque, IA). All the solutions were prepared and the experiments were conducted using Nanopure water.

3.2.2. *Surfactant Purification*

Surfactants may contain trace amount of their more surface-active parent components (47, 48). These more surface-active parent components preferentially remain in surfactant adsorbed layers (47, 48). A foaming technique was used to get rid of these trace amount of their more surface-active parent components before using the surfactants in this study. Pure N_2 gas was sparged through the surfactant solution to produce foam (Figure 3.4).

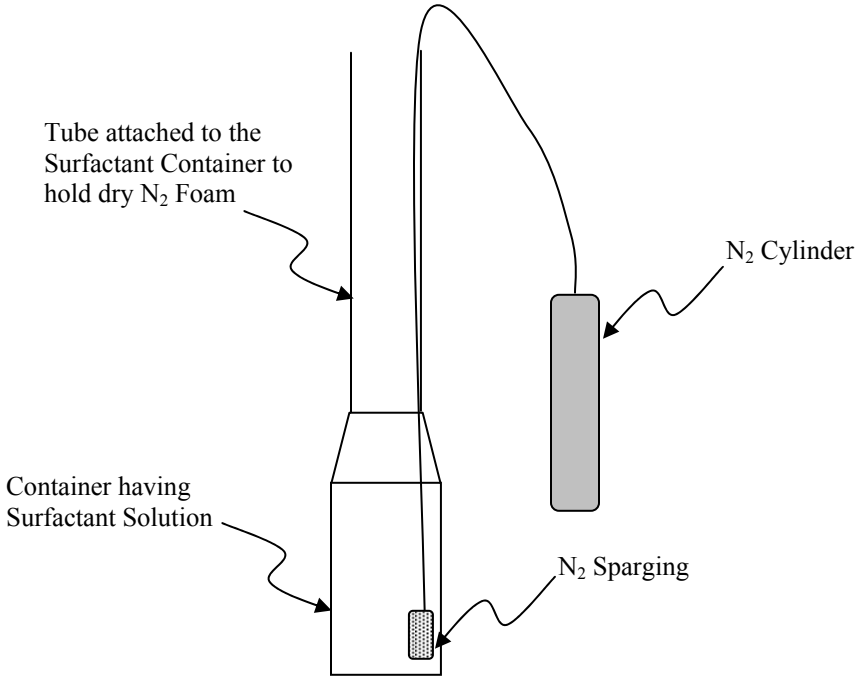

Figure 3.4: Schematic diagram of Surfactant purification

After 30~40 minutes of foaming, the dry foam was removed and surfactant solution was carefully collected from the bottom of the container. The surfactant

concentration changes because of foam removal. So the concentration of purified surfactant was measured using UV spectrophotometer.

3.2.3. *Experimental Procedures: Expansion Experiments*

Surfactant pendant drop was formed in the air and was expanded by pumping solvent into the drop over a short period of time. Experiments were conducted in a customized 4.5 cm × 4.5 cm × 3 cm closed optical cell (Figure 3.5). The optical cell is designed to access by opening the side glass panel. A metal tube is attached at the top of the cell. The metal tube is connected to a syringe pump by $\frac{1}{16}$" outside diameter (OD) HPLC tubing. The syringe pump is used to pump Nanopure water at different controlled flow rate through the HPLC tubing. The purpose of the vertical metal tube is to provide a smooth tip for the pendant drop so that the drop will be symmetrical with respect to vertical axis. Experiments were conducted in two parallel experimental setups similar to one described Section 2.3.2 (43) (Figure 2.5). Only the optical cell was replaced with the one shown in Figure 3.5.

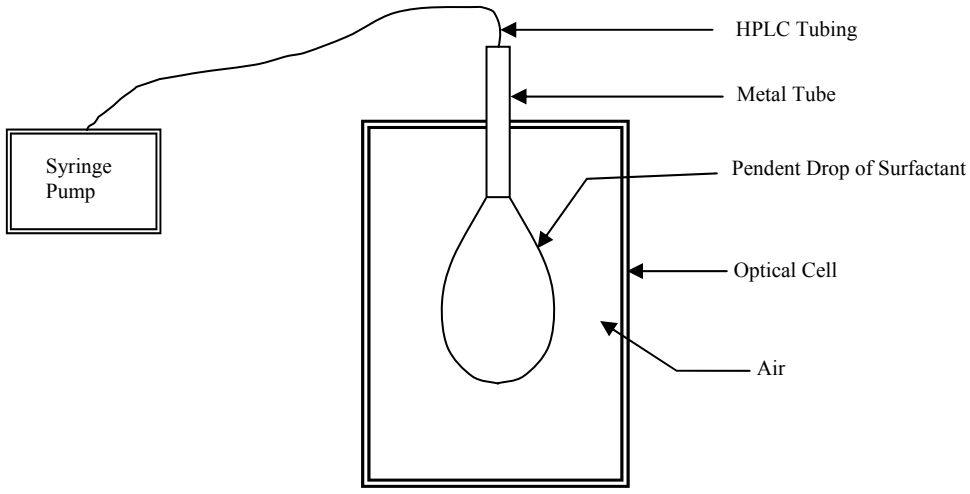

Figure 3.5: Schematic diagram of closed optical cell. View of pendent drop of surfactant solution.

First the camera is focused by using a precision sphere. Initially a very small volume (1~1.5 μL) of Nanopure water is pumped at the tip of the metal tube. The pump is then stopped and the camera is turned on to start capturing image at a certain interval. A small volume (about 5uL) of known high concentration surfactant solution is injected into the Nanopure water (1~1.5 μL) drop by using a 10 μL syringe. After forming the high concentration (5~7) μL pendant drop at the tip of the metal tube, the syringe pump is turned on to pump the Nanopure water into the high concentration surfactant drop. Over time, the drop volume increases and the drop concentration decreases due to continuous Nanopure water pumping. The images captured over time are stored in the computer and are later analyzed by using customized software written for the purpose.

3.2.4. *Pendant Drop Analysis*

Drop volume and interfacial tension were measured using axisymmetric drop shape analysis (13, 33, 34, 35). Edge detection was done using the Sobel edge operator (33), and drop profiles were fit using a fourth order Runge-Kutta solution of the Bashforth-Adams equation (4) and nonlinear regression fits based on the Nelder- Mead downhill-simplex algorithm (36). Automated software written for this purpose was used to analyze batches of hundreds of images.

3.2.5. *Dilution Model*

Based on the hypothesis, adsorption of surfactant at freshly formed surface/interface is rapid compared to diffusion/mixing; a numerical model was solved by solving 1D diffusion equation. The model is used to predict actual instantaneous concentration of surfactant at the freshly formed pendant drop surface/interface.

The objective is to model the concentration distribution in drop over time in course of dilution. During dilution, the pendant drop is assumed to have a well mixed core at the center and a stagnant boundary layer having concentration gradient (low to high from well-mixed core to outward or air/water surface). A schematic diagram of the hypothetical dilution scenario has been shown in Figure 3.6.

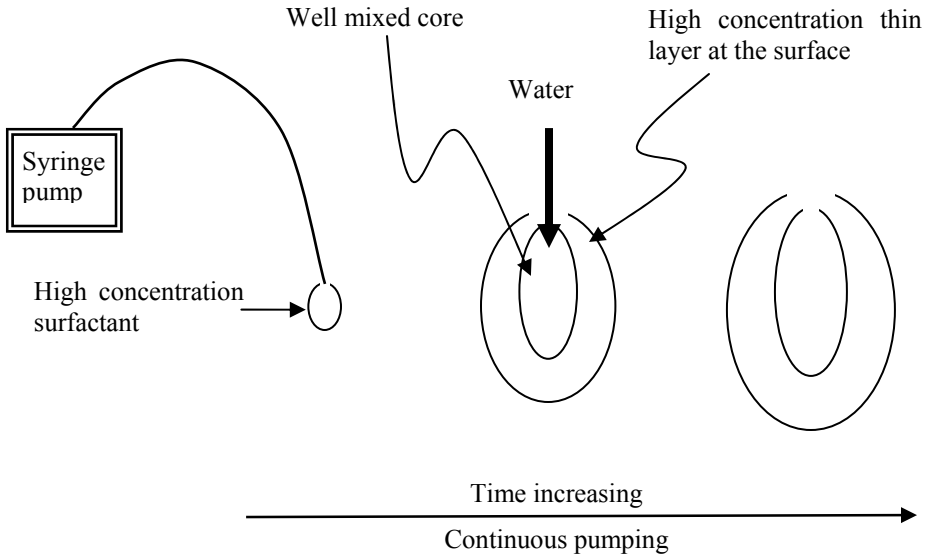

Figure 3.6: Schematic diagram of hypothetical dilution scenario of a pendent drop.

As the high concentration layer at the surface of the pendent drop is microscopically thin, considering the layer as a 1-D domain is appropriate for predicting surfactant concentration at the surface of the pendent drop. The governing equation to describe diffusion/mixing of surfactant is (49):

$$\frac{\partial C}{\partial t} = D\frac{\partial^2 C}{\partial x^2} \tag{3.4}$$

Where , C = concentration of surfactant,

t = time,

D= diffusion (mixing) coefficient and

x = distance along the concentration gradient layer.

- The differential equation was solved using backward euler approximation in time and forward difference approximation in space. The initial and boundary conditions used to solve the equation are:

  Initial condition, $C(x, t=0) = C_0$. C_0 is the initial concentration of the drop just after surfactant injection and prior to dilution.

  Boundary Conditions, $C(x=0, t=0) = C_0$ and $\frac{\partial C}{\partial x}|_{(x=L)} = 0$. L is the length of the concentration gradient layer.

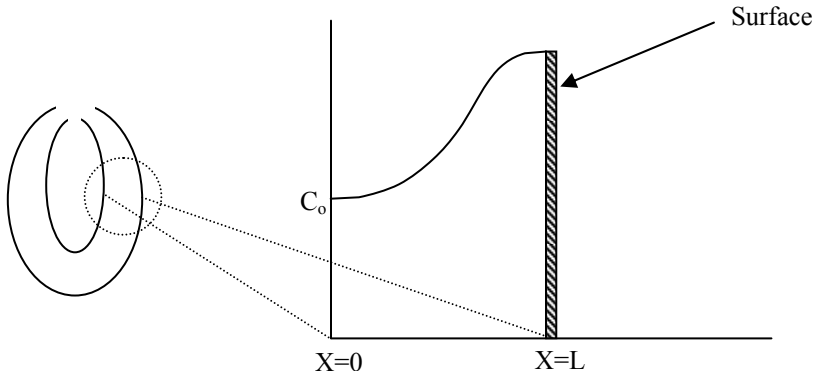

Figure 3.7: Setting model parameter to calculate the concentration gradient in the high concentration thin layer (at the surface of the pendent drop).

In the dilution experiment, as water is continuously pumped into the surfactant pendent drop, a mechanical mixing takes place inside the drop. So molecular diffusion is not the only driving force for surfactant molecules to move from high concentration thin layer to well mixed core of the drop. To account for the mechanical mixing, a mixing

coefficient instead of molecular diffusion coefficient has been used to solve the diffusion equation.

A dimensionless π-parameter as a function of diffusion/mixing coefficient (D), Volume (V), pumping flow rate (Q) and characteristic length taken as tube radius (R) was derived.

$$\pi = \frac{D^2 \times V}{R \times Q^2} \tag{3.5}$$

The model requires initial concentration (C_0), initial volume of the drop (V_0), final volume (V_f), pumping flow rate (Q), π parameter, length of concentration gradient layer (L) and characteristic length taken as tube radius (R) as inputs and the model can calculate the concentration distribution in the drop over time. The π parameter was used to adjust the diffusion/mixing coefficient (D) due to change of volume in course of dilution.

3.3. RESULTS AND DISCUSSION

During dilution, as Nanopure water is pumped into the surfactant pendant drop, the volume of the drop increases and average concentration of the drop decreases over time. So the surface tension of pendant drop should increase with the decrease in concentration (e.g. Figure 3.3). But when surface tension (in course of dilution) was plotted against average concentration (the mass of surfactant in the drop divided by the instantaneous volume of the drop), the surface tension curve did not follow the traditional surface/interfacial tension curve. Instead they exhibited lower interfacial tension compared to the traditional surface tension at same average concentration (Figure 3.8).

Traditional surface/interfacial tension curve is a plot of surface/interfacial tension vs. well-mixed and equilibrium concentration of surfactant (e.g. Figure 3.3). In this study, different concentration of surfactant solution was first prepared. Then pendant drop method (4) was used to measure surface tension of the surfactant at different concentration. Then surface tension data were plotted as a function of well-mixed concentration to get a traditional surface/interfacial tension curve.

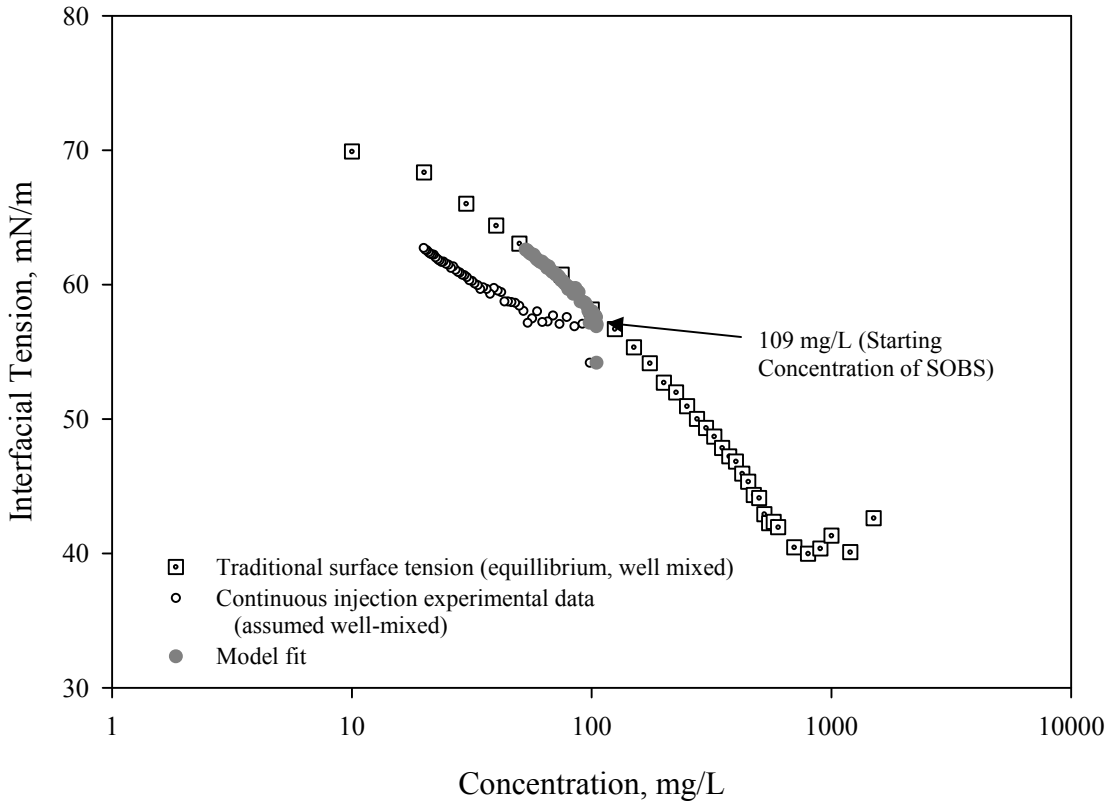

Figure 3.8: Interfacial tension of SOBS + 0.1 M NaCl at different concentration during 0.1 M NaCl pumping [Average pumping rate ~ 3.89 μL/ min]

In Figure 3.8, the traditional surface tension curve represents equilibrium surface tension of SOBS+0.1M NaCl at different concentration. And the continuous injection experimental data represents the surface tension of SOBS+0.1M NaCl in course of

dilution due to continuous injection of 0.1M NaCl into the surfactant pendant drop. The starting point concentration (prior to dilution by pumping 0.1M NaCl) of SOBS was 109 mg/L and the corresponding surface tension matched the equilibrium surface tension of SOBS.

During continuous injection of 0.1M NaCl (0.1M NaCl was pumped to keep the salt concentration in the pendant drop constant in course of dilution) the pendant drop was assumed well-mixed and surface tension was plotted as a function of average concentration (measured from change of volume of pendant drop) of SOBS. But during dilution instead of following equilibrium surface tension curve, the dynamic surface tension data (due to continuous injection of 0.1M NaCl) were lower compared to equilibrium surface tension and followed a different curve (Figure 3.8). Considering this experimental data, it was hypothesized that during dilution, adsorption of SOBS at the air/water interface is faster than diffusion/mixing. That means when 0.1M NaCl was pumped into the surfactant pendant drop, as volume increased at every instant, a well-mixed core (diluted SOBS concentration) was formed at the center of the pendant drop and a layer having concentration gradient (low to high from center to the air/water surface) was developed due to lack of mixing compared to faster adsorption of high concentration SOBS at the freshly formed air/water surface, that lowered the instantaneous surface tension than the equilibrium surface tension.

In Figure 3.8, initial SOBS concentration was 109mg/L. By adjusting the π parameter ($\pi=7x10^{-7}$ gives the best fit), the dilution model successfully able to model the experimental data to follow equilibrium surface tension curve (Figure 3.8).

Figure 3.9 shows modeling of the entire concentration range of equilibrium surface tension data for SOBS below CMC.

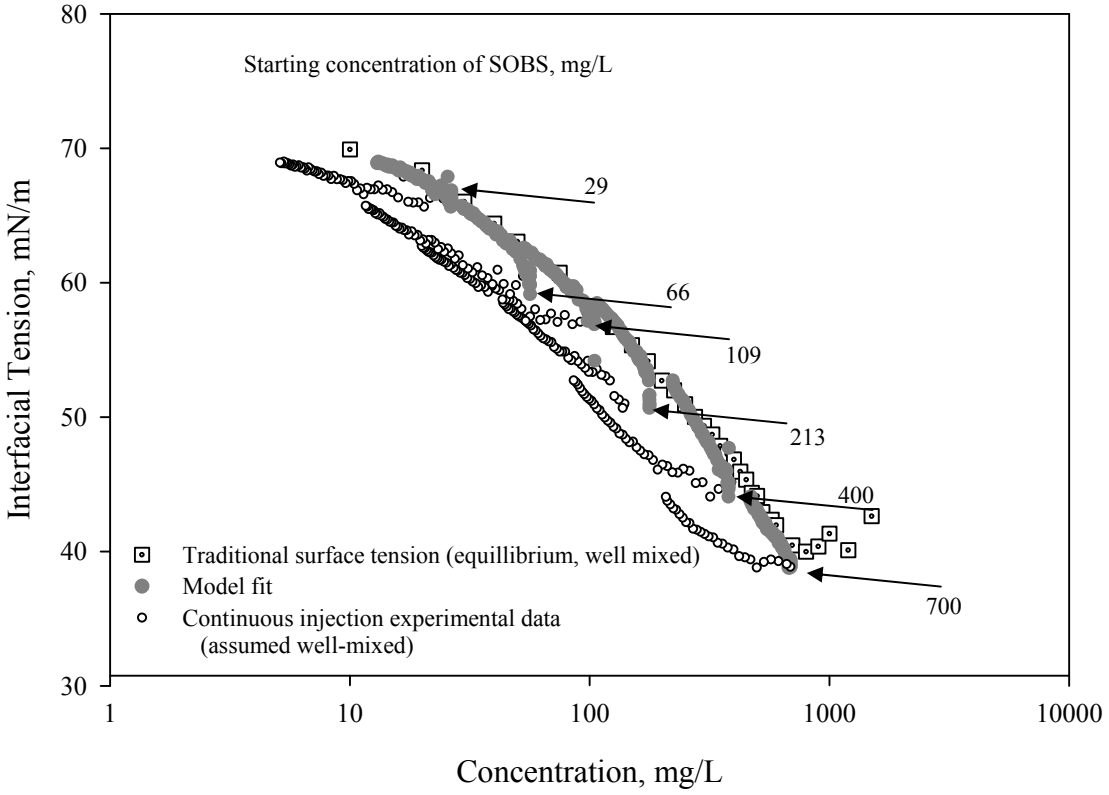

Figure 3.9: Interfacial tension of SOBS + 0.1 M NaCl at different concentration during 0.1 M NaCl pumping [Average pumping rate ~ 3.89 μL/ min]. Six different initial concentration SOBS solution was used to cover the entire IFT curve.

Six different concentrations of surfactant drop were required to cover the entire concentration range of equilibrium surface tension curve of SOBS. For every initial concentration of SOBS same π parameter ($7x10^{-7}$) was used to adjust mixing coefficient due to volume change.

Pumping flow rate of 0.1M NaCl was also varied to check the flow rate dependency of the model. Three different flow rates (3.9 μL/min, 7.6 μL/min and 15 μL/min) were used for the entire range of SOBS concentration (below the CMC).

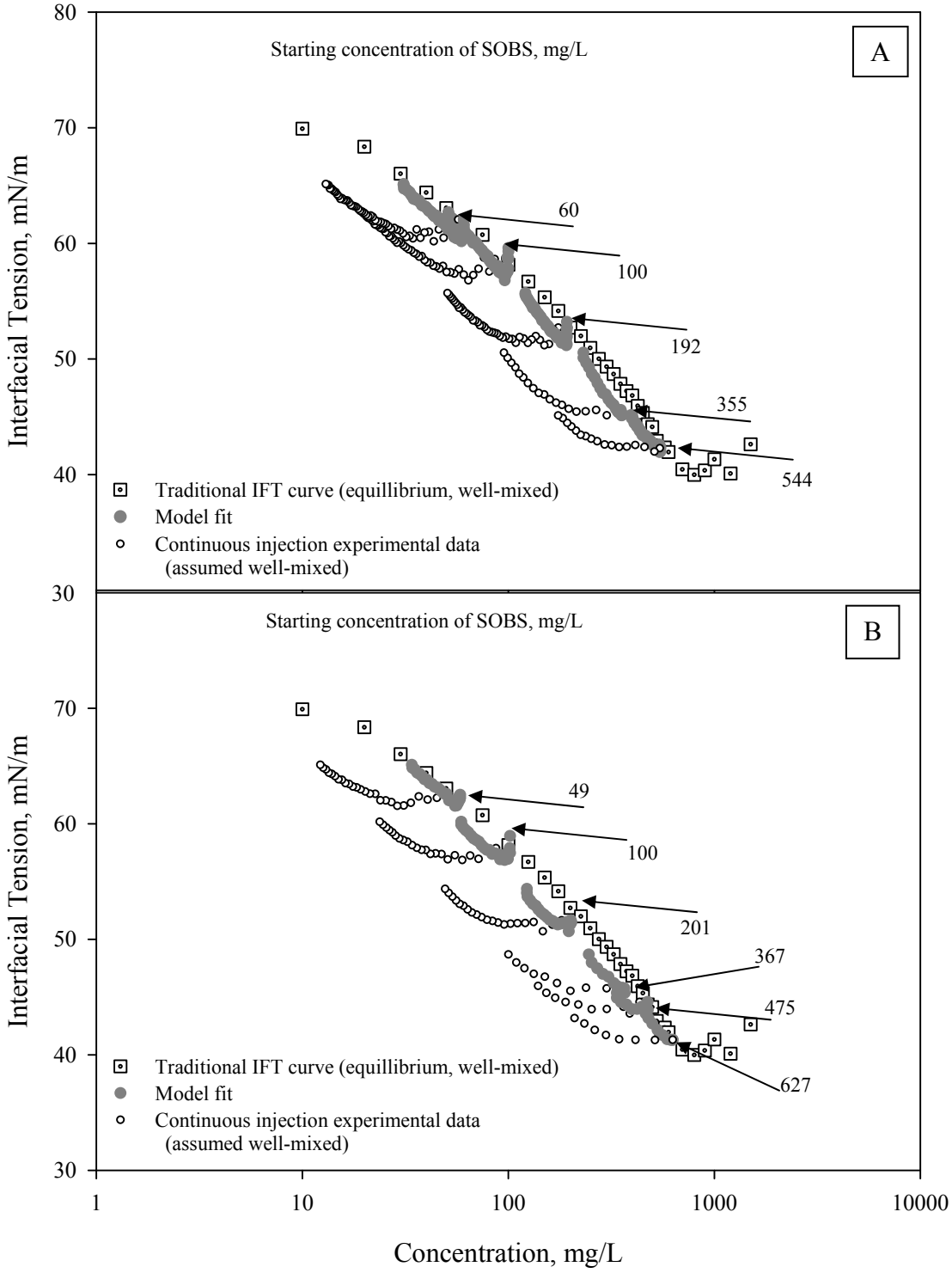

Figure 3.10: Interfacial tension of SOBS + 0.1 M NaCl at different concentration during 0.1 M NaCl pumping [Average pumping rate 7.6 μL/ min (A) and 15 μL/ min (B)]. Five (A) and six (B) different initial concentration SOBS solution was used to cover the entire IFT curve.

Figure 3.9 and 3.10 (A, B) show the modeling of dynamic surface tension of SOBS in which 0.1M NaCl was pumped at 3.9 μL/min, 7.6 μL/min and 15 μL/min respectively. For all three pumping flow rates, the dilution model was able to model dynamic surface tension of SOBS using the same π parameter ($7x10^{-7}$). So the use of π to modify mixing coefficient (D) allows the model to describe the mixing behavior at different flow rates. Flow rate greater than 15 μL/min produced pendant drops that were too unstable for reliable surface tension measurement from axisymmetric drop shape analysis.

Figure 3.11 shows the application of the model for the dilution of a cationic surfactant, CPC at three different flow rates. Figure 3.11 (A) shows dynamic surface tension at pumping flow rate 3.9 μL/min, Figure 3.11 (B) shows dynamic surface tension at pumping flow rate 7.6 μL/min and Figure 3.11 (C) shows dynamic surface tension at pumping flow rate 15 μL/min. For all three cases, same π parameter (7E-7, same as SOBS) was used. One interesting thing to be noted that for SOBS and CPC, the diffusion model parameters (initial volume, final volume, initial concentration, pumping flow rates) were different for each set of experiments and same π parameter was able to scale the mixing coefficient to calculate surfactant concentrations.

Another interesting observation was made in Figure 3.11. The starting surface tensions (just after pumping started) were higher than the equilibrium surface tension and later, in course of dilution, the dynamic surface tension reduced and matched equilibrium surface tension. As for example in Figure 3.11-C for initial concentration of 118 mg/L, starting surface tension was ~61 mN/m but later it reduced to 58 mN/m and matched equilibrium surface tension.

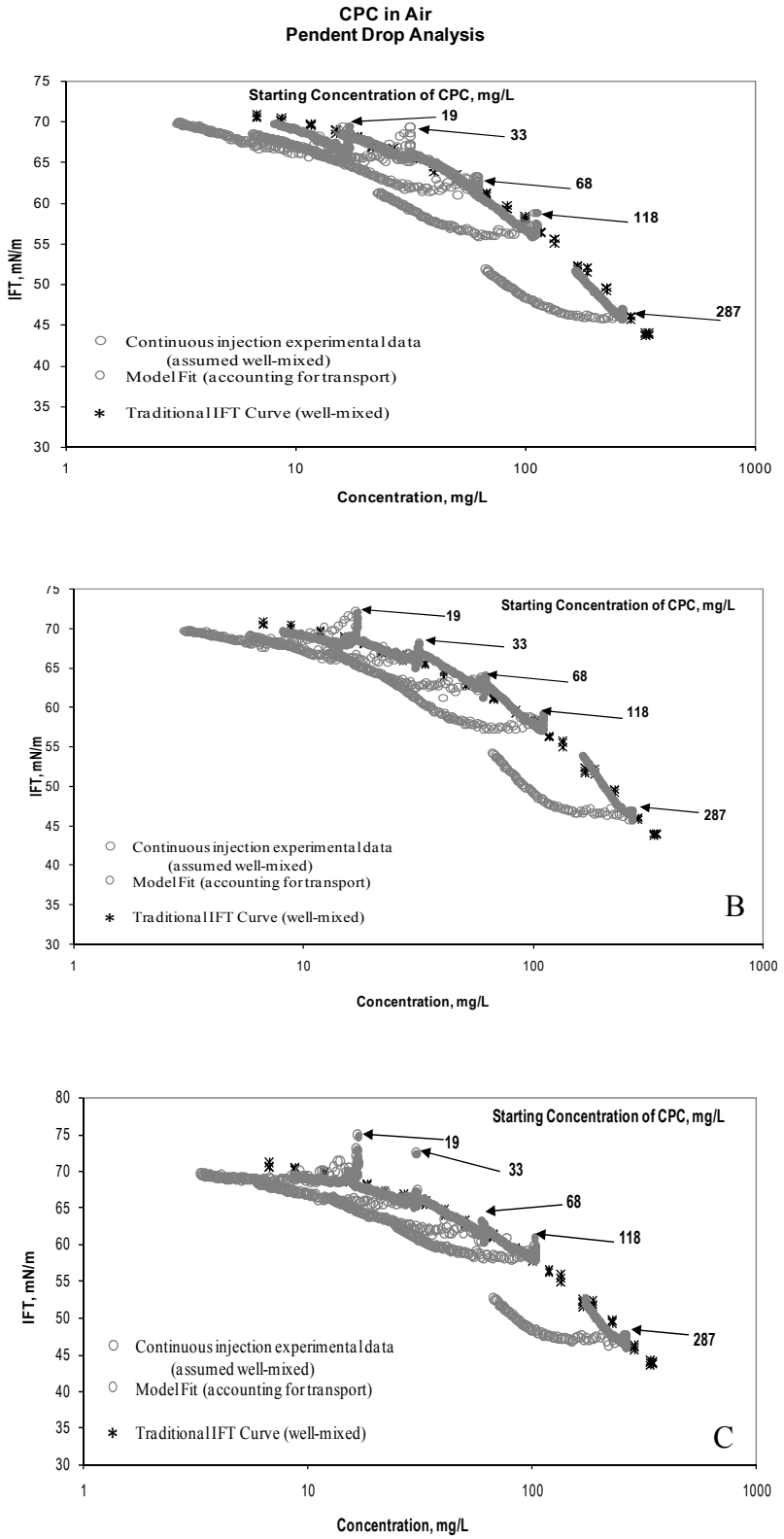

Figure 3.11: Interfacial tension of CPC at different concentration during nanopure water pumping [Average pumping rate A: 3.8 µL/ min, B: 7.6 µL/ min and C: 15 µL/ min]. Five different initial concentration CPC solutions were used to cover the entire IFT curve.

A probable explanation to this scenario is, when a fresh surface of water formed, theoretically the surface tension should be ~72 mN/m and as surfactant starts to adsorb, surface tension decreases. At the beginning of the dilution experiment, when pumping started, the image corresponding to 61 mN/m drop might not have sufficient amount of surfactant adsorbed to attain equilibrium surface tension (58 mN/m) and later, when adequate surfactant monomer adsorbed, the surface tension reduced to equilibrium surface tension. If it was possible to image expanding drops fast enough (prior adsorption started) then starting surface tension could be ~72 mN/m.

Figure 12 shows the application of the model for a nonionic surfactant, NP15. By adjusting the π parameter, the dilution model failed to model the experimental data to follow the equilibrium surface tension curve of NP15. One possible reason is that NP15 takes a long time to attain equilibrium surface tension. In that case the equilibrium surface tension curve (measured using pendant drop technique in air) may not give the true equilibrium surface tension. Because to get true equilibrium surface tension the pendant drop is required to hold for sufficiently long time. And that may lead to a considerable amount of volume loss by evaporation. To eliminate this issue of volume loss, traditional surface/interfacial tension curve for NP15 was regenerated by using air bubble. In this method, air bubble was formed in different concentrations of NP15 surfactant and was held for over 20 minutes (for each concentration). Interfacial tension of NP15 was plotted as a function of time to check attaining equilibrium surface/interfacial tension. 20 minutes found to be sufficient to attain equilibrium surface/interfacial tension for all the concentrations. Traditional surface/interfacial

tension curve from bubble method found to be quite different compare to pendant drop method (Figure 3.12).

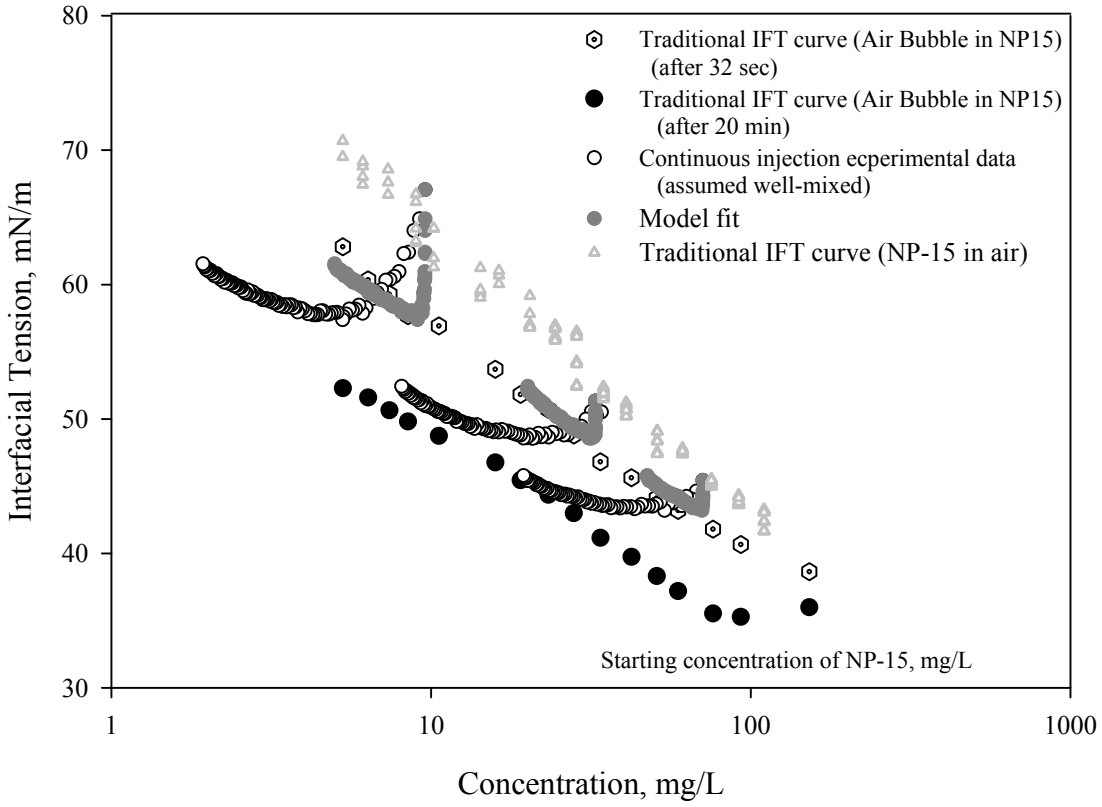

Figure3.12: Interfacial tension of NP-15 at different concentration during dilution [Average pumping rate 3.8 μL/ min].

For each concentration of NP15, surface/interfacial tension is much lower in bubble method (after 20 minutes) compared to pendant drop method. So, it is safe to assume NP15 takes longer time to reach equilibrium surface/interfacial tension. But unfortunately the model fit data did not follow the traditional curve using bubble method. Instead, the model fit data followed a curve in between two traditional surface/interfacial tension curves (Figure 3.12). In bubble method, interfacial tension data was available

ranging from 0 to 30 minutes at certain time interval. After some trial, the model fit data were showing good match with the traditional surface/interfacial data after 32 seconds (Figure 3.12). As NP15 takes longer time to attain equilibrium surface tension, when Nanopure water was continuously injected to NP15 during dilution, adsorption was not fast enough to match traditional curve from pendant method and again due to continuous injection, NP15 was not getting enough time to adsorb on the newly formed surface to match traditional curve due to bubble method. Instead, NP15 model fit data was able to match traditional curve formed after 32 seconds.

3.4. CONCLUSIONS

Diffusion/mixing plays a key role in surface/interfacial tension modification of surface/interfaces. From the modeling of CPC and SOBS data, it is apparent that surface/interfacial tension modification of surface/interfaces is diffusion/mixing rate limiting in case of the cationic and anionic surfactants studied. But in case of nonionic surfactant, it can be assumed that initially the equilibration was adsorption rate limiting and after certain time (in case of NP15 it was 32 seconds) the surface/interfacial tension modification of surface/interfaces becomes diffusion/mixing rate limiting. Further experiments with other nonionic surfactants are required to have a better understanding of the dynamics of interface equilibration processes. This study can also become the basis of the development of a rapid method of surface/interfacial tension curve for different types of surfactant.

CHAPTER 4

DYNAMICS OF INTERFACIAL ADSORPTION DURING DROP EVAPORATION

4.1. INTRODUCTION

In the work described in this chapter, the dynamic surface/interfacial tension of surfactant solution has been studied during drop evaporation and compared with the equilibrium surface tension to understand the dynamics of surface/interfacial adsorption to a contracting surface. As evaporation of a surfactant drop takes place, the drop loses volume and the air-surfactant surface shrinks. At the same time, the average concentration of the drop increases continuously due to the reduction in volume. Two processes take place simultaneously on the surfactant drop in the course of evaporation: (i) Adjustment of the adsorption equilibrium as interface contracts and releases surfactant to the solution and (ii) Diffusion of surfactant from surface to drop solution. If the surface contraction (due to evaporation) and releases surfactant to the solution is rapid compared to diffusion of surfactant, then the surface concentration of the drop will be higher than the average concentration. This will cause the instantaneous surface tension of the drop (in the course of evaporation) to be lower than the equilibrium surface tension.

Two different surfactants have been used to study the dynamic surface/interfacial tension in the course of evaporation. Two different numerical models have also been developed to get a better understanding of the dynamics of surface/interfacial adsorption to a contracting surface.

4.2. MATERIALS AND METHODS

4.2.1. *Materials*

Surfactants used in this study are one cationic surfactant, cetylpyridinium chloride (CPC), and one nonionic surfactant, a polydisperse commercial nonylphenol ethoxylate, Tergitol NP15. CPC was purchased from Sigma-Aldrich Co. (St. Louis, MO), and NP15 was donated by DOW (Midland, MI). All the chemicals had stated purities of 99% or higher. All the glassware were cleaned prior to use by rinsing in HPLC-grade methanol (Sigma-Aldrich), soaking for 24 h in 1% LIQUI-NOX solution (Alconox, Inc., White Plains, NY) followed by at least 10 rinses in Nanopure water (Barnstead, Dubuque, IA). All the solutions were prepared and the experiments were conducted using Nanopure water.

4.2.2. *Surfactant Purification*

Surfactants contain trace amount of their more surface-active parent components (17, 18). These more surface-active parent components preferentially remain in surfactant adsorbed layers (17, 18). A foaming technique was used to get rid of these trace amount of their more surface-active parent components before using the surfactants in this study. Pure N_2 was sparged through the surfactant solution to produce foam (Figure 3.4). Details of this procedure have been described in Section 3.2.2 of Chapter 3.

4.2.3. *Experimental Procedures: Drop Expansion Experiments*

Surfactant solution pendant drops ware formed in the air and allowed to evaporate undisturbed over a short period of time. Experiments were conducted in open air at room

temperature **(Figure 4.1)**. In Figure 4.1 a metal tube is attached at the top of the metal stand. The metal tube is connected to a syringe pump by $\frac{1}{16}$" outside diameter (OD) HPLC tubing. A syringe pump is used to pump low concentration surfactant at uniform flow rate through the HPLC tubing to form the drop. The purpose of the vertical metal tube is to provide a smooth tip for the pendant drop so that the drop will be symmetrical with respect to the vertical axis. Experiments were conducted in two parallel experimental setups similar to the one described Section 2.3.2 (19) (Figure 2.5) except the optical cell was replaced with the setup shown in Figure 4.1.

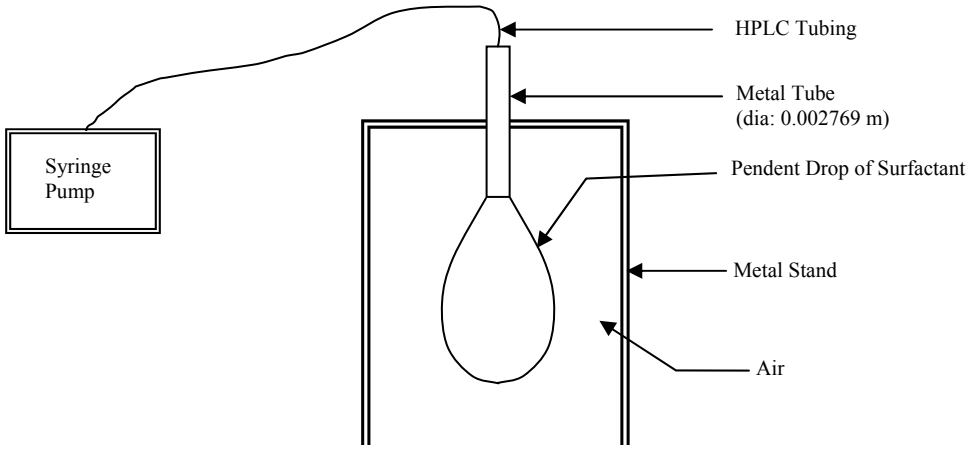

Figure 4.1: Schematic diagram of evaporation of a pendent drop of surfactant solution.

First the camera is focused by using a $\frac{1}{8}$" precision sphere. The camera will be turned on to capture images at a certain time interval. Initially a low concentration of surfactant solution will be pumped to form a large pendent drop. The pump will be stopped and the drop will be left undisturbed to evaporate. The images captured over

time are stored in the computer and later analyzed by using customized software written for the purpose.

4.2.4. *Pendant Drop Analysis*

Drop volume and interfacial tension was measured using axisymmetric drop shape analysis (13, 20, 21, 22). Edge detection was done using the Sobel edge operator (20), and drop profiles were fit using a fourth order Runge-Kutta solution of the Bashforth-Adams equation (3) and nonlinear regression fits based on the Nelder- Mead downhill-simplex algorithm (23). Automated software written for this purpose was used to analyze batches of hundreds of images.

4.3. EVAPORATION ANALYSIS

Two different models were used to explore the dynamics of surface/interfacial adsorption of surfactant to a contracting surface in the course of evaporation. The models were used to predict the actual instantaneous concentration of surfactant at the contracted pendant drop surface in the course of evaporation.

4.3.1. *Evaporation Model #1*

In Evaporation Model #1, the surface region of surfactant pendant drop was considered as a 1-D infinite domain and the numerical model was solved by solving 1-D diffusion equation. This model uses a 1-D finite diffusion solution to the diffusion equation, with a re sampling technique to a handle the moving boundary (contracting interface). A schematic diagram of the hypothetical evaporation scenario has been shown in Figure 4.2. Note that the assumption of an infinite domain with a well-mixed core

means this model should work best for short times at the onset of diffusion (before the core concentration begins to increase).

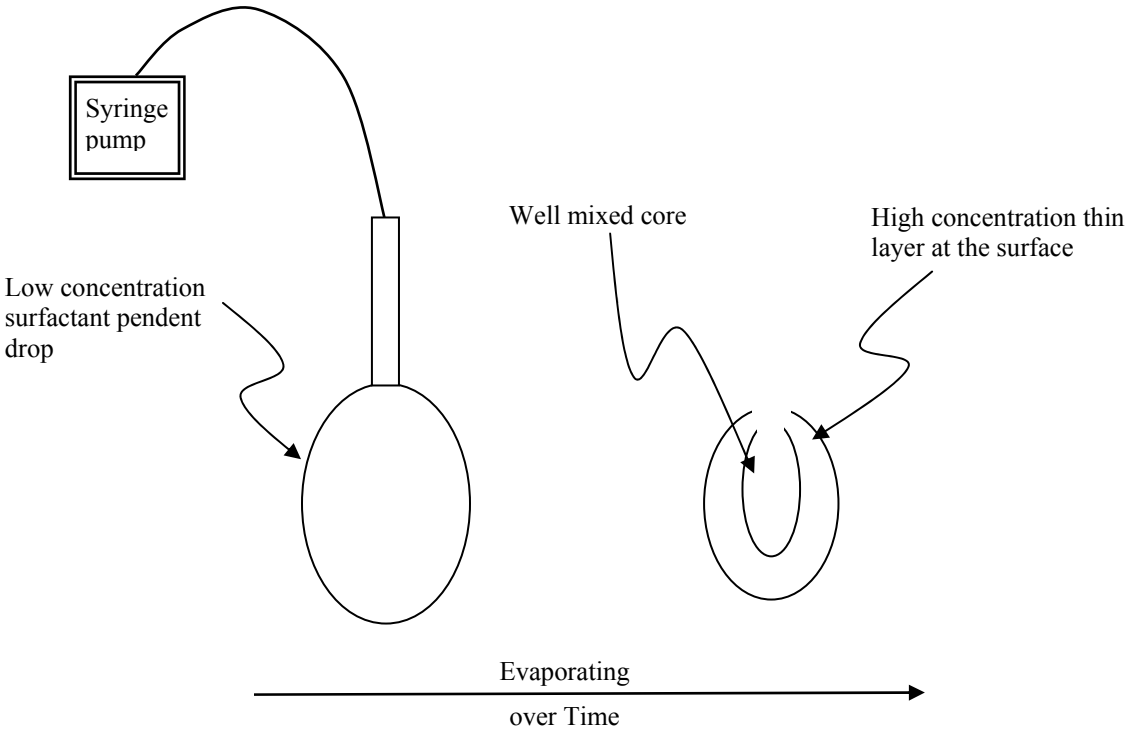

Figure 4.2: Schematic diagram of hypothetical evaporation scenario of a pendent drop.

The high concentration layer at the surface of the pendent drop is considered as a 1-D domain to solve the evaporation model. The governing equation to describe diffusion of surfactant is (24):

$$\frac{\partial C}{\partial t} = D\frac{\partial^2 C}{\partial x^2} \tag{4.1}$$

Where, C = concentration of surfactant,

t = time,

D = diffusion (molecular) coefficient and

x = distance along the concentration gradient layer.

The differential equation was solved using backward euler approximation in time and central difference approximation in space. The initial and boundary conditions used to solve the equation are:

Initial condition, $C(x, t=0) = C_0$. C_0 is the initial concentration of the drop just after formation of the surfactant pendent drop prior evaporation (Figure 4.3).

Boundary Conditions, $\frac{\partial C}{\partial x}|_{(x=0)} = 0$ and $\frac{\partial C}{\partial x}|_{(x=L)} = 0$. L is the length of the concentration gradient layer (Figure 4.3).

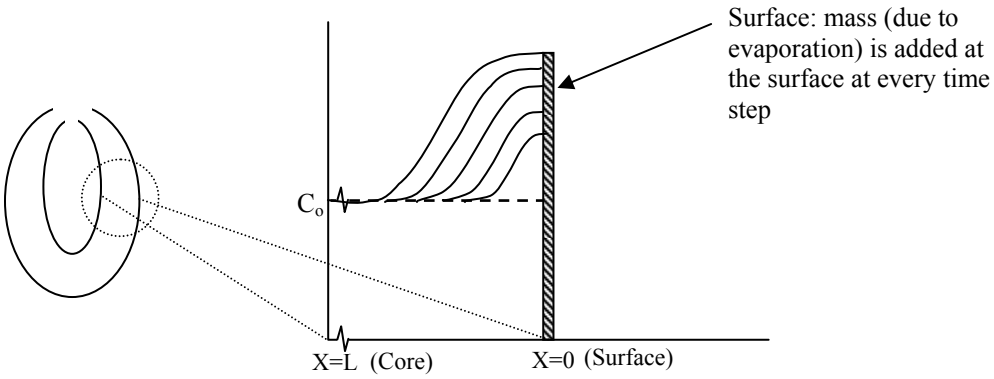

Figure 4.3: Setting model parameter to calculate the concentration gradient in the high concentration thin layer (at the surface of the pendent drop).

The increase of concentration (due to loss of volume) is added at x = 0 ($C_{(x=0, t)}$) at every time step. So $C_{(x=0, t)}$ is considered as constant boundary condition but modified at every time step. The model works until the drop has shrunk to the point that the concentration in the core (x=L) begin to increase. So the diffusion equation was solved

for functionally infinite domain by making "L" large enough that the boundary condition at x=L does not influence the solution (or, C(x=L, t) = C_0).

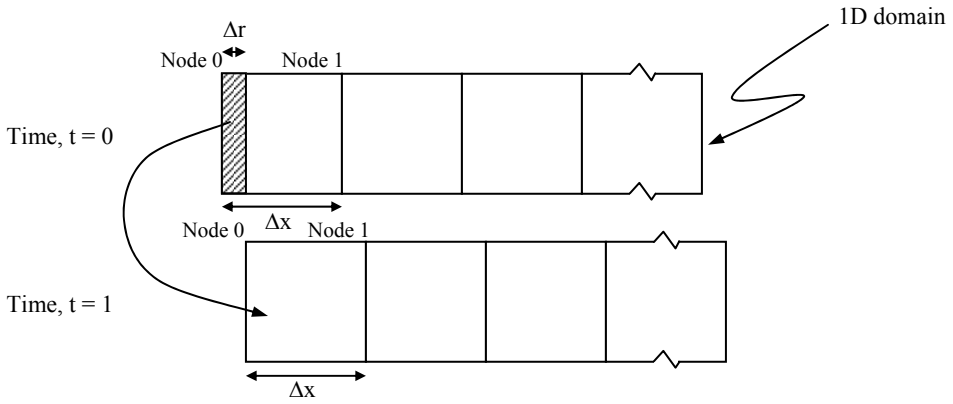

Figure 4.4: Increase of concentration (due to loss of volume), added at x = 0 (node 0), ($C_{(x=0,\ t)}$). Δr: length evaporates at any time, t; Δx: length of each node.

Figure 4.4 shows a schematic diagram of handling initial concentration (C_0) and shift of node at every time step. Δr: length evaporates at any time, t and is calculated from change of volume over time t. Δx: length of each node of the 1D domain. So concentration of surfactant at any node at any time step t can be calculated by using equation (4.2), (4.3) and (4.4).

$$C_{(j,t)} = (1-f) * C_{(j,t-1)} + f * C_{(j+1,t-1)} \tag{4.2}$$

$$C_{(0,t)} = C_{(0,t-1)} + f * C_{(1,t-1)} \tag{4.3}$$

Where, $$f = \frac{\Delta r}{\Delta x} \tag{4.4}$$

The model requires initial concentration (C_0), initial volume of the drop (V_0), final volume (V_f), evaporation rate (volume change rate (Q)), molecular diffusion coefficient (D) and length of concentration gradient layer (L) as inputs and the model can calculate the concentration-distribution in the drop over time.

4.3.2. *Evaporation Model #2*

In Evaporation Model #2, the pendant drop was considered as a sphere and the radius of the sphere is considered as the length of the 1-D domain to solve the model using 1-D diffusion equation. This model was developed to model later time data where zone concentration is increasing.

In this model, the surfactant pendant drop radius is considered as the 1D domain to solve the evaporation model using 1D diffusion equation. To keep the calculation simple, the pendant drop is considered as a sphere to calculate the radius (R) of the drop. Figure 4.5 shows the schematic diagram of the model to understand the setting of model parameter. Contrary to the previous model, entire radius of the pendant drop has been used as a 1D domain in this model (instead of a layer of high concentration surfactant at the surface). So in the course of evaporation, as volume changes, the length of the 1-D domain (or radius of the drop) changes and concentration distribution (mass of surfactant) in the nodes along the 1-D domain must be re-sampled at every time steps.

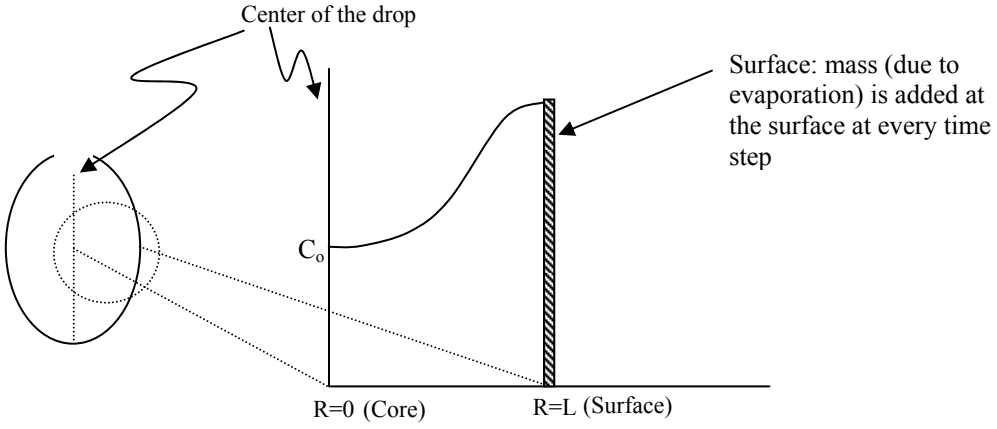

Figure 4.5: Schematic diagram of Model #2.

Governing equation to describe diffusion of surfactant is same as previous model (equation 4.1). The initial and boundary conditions to solve the equation 4.1 also remain the same as described in section 4.3.1 (although in this case the ends are reversed and node 0 is at the core of the drop (Figure 4.5, 4.6)). The difference is the re-sampling of the surfactant concentrations (due to evaporation) in the nodes of the 1D domain. Unlike previous model, the length between nodes (Δx in previous model) changes as the number of nodes remains same through out the solution.

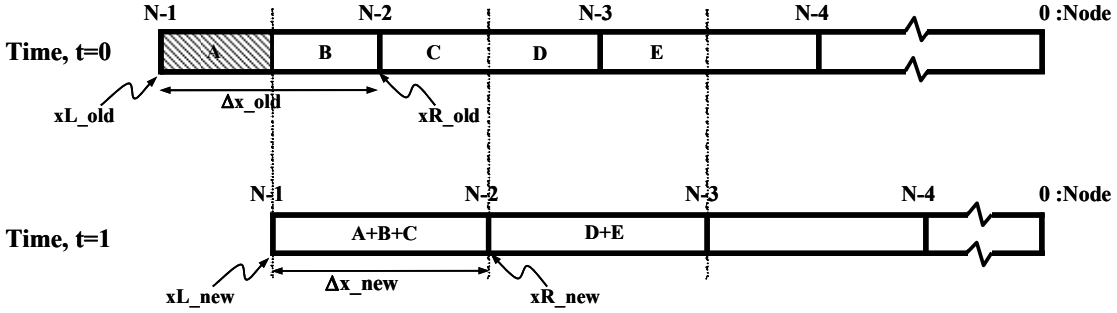

Figure 4.6: Schematic diagram of 1D domain to show the surfactant concentration re-sampling (due to evaporation). Node (N-1) is the surface; Node 0 is the core (center of drop). A: evaporating length, corresponding mass is added to xL_new. B, C: overlapped portion contributed to Δx_new.

Figure 4.6 shows the schematic diagram of handling the redistribution of surfactant concentration (mass) due to evaporation. Note that: Δx is changing over time due to reduction of radius of pendant drop ($\Delta x\_old \neq \Delta x\_new$). Mass of surfactant at portion A, B and C in Figure 4.6 will contribute to the concentration at N-1 node after evaporation. For any node or segment, the length of the overlapped portion (i.e.: B,C for N-1/N-2 section ; D&E for N-2/N-3 section) is required to first calculate to get the

redistributed concentration after evaporation. Then redistributed concentration can be calculated by using equation 4.5.

$$C_{new}[i] = \sum C_{old}[j] * \frac{OL}{\Delta x\_new} \tag{4.5}$$

Where, OL = overlapped lengths.

i = node of the new domain (after evaporation)

j = nodes corresponding to the overlapped portion of the old domain (before evaporation)

For the surface node (N-1), evaporated portion also required to be added with the overlapped portion:

$$C_{new}[N-1] = C_{new}[N-1]_{(overlappedportion\ using\ equation\ 4.5)} + \frac{(\Delta x\_old - OL)}{\Delta x\_new} * C_{old}[N-1] \tag{4.6}$$

This re-sampling of concentration is performed in every time steps before using diffusion equation to describe the diffusion of surfactant.

4.3.3 *Results and discussion*

During evaporation, as the surfactant pendant drop loses solvent, volume of the drop decreases and average concentration of the drop increases over time. Figure 4.7 shows the evaporation of a CPC pendant drop in air over approximately 30 minutes. In the course of evaporation, the CPC drop volume decreased from 37.4 μL to 23.8 μL, and the measured interfacial tension decreased from 59.6 mN/m to 45.9 mN/m.

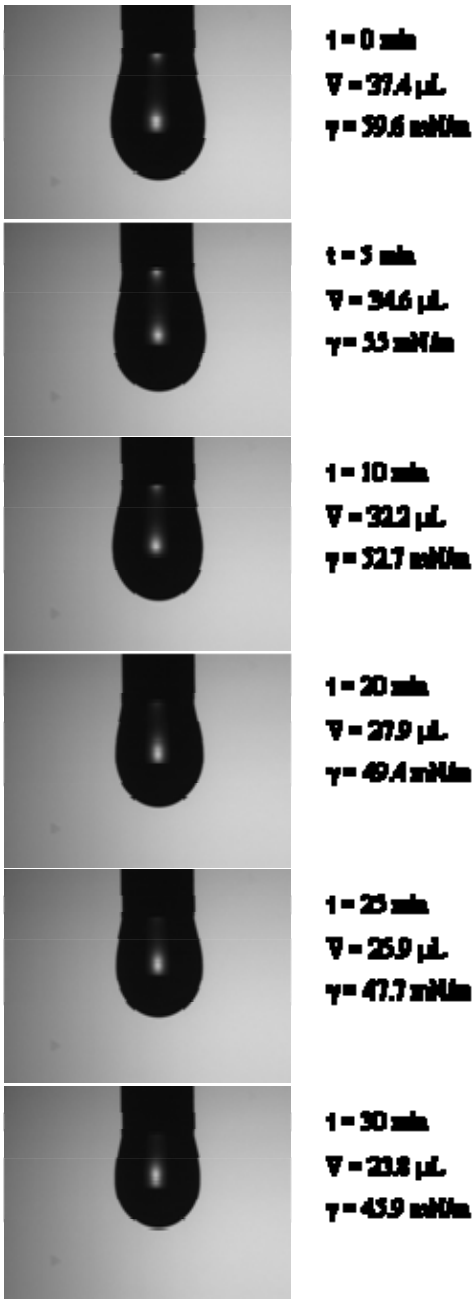

Figure 4.7: Evaporation of CPC pendant drop in air over approximately 30 minutes. Time (t), drop volume (V), and surface tension (γ) are indicated.

Figure 4.8 shows the interfacial tension of CPC as a function of concentration. In Figure 4.8 the traditional surface tension curve represents equilibrium surface tension of CPC at different concentration. And the experimental data in the course of evaporation

represents quantitative analysis of the experimental data corresponding to the images shown in Figure 4.7. The starting point concentration (prior to evaporation) of CPC was 40 mg/L and the corresponding surface tension matched the equilibrium surface tension of CPC. During evaporation the pendant drop of CPC was assumed to have uniform concentration (concentration was calculated from the mass of surfactant in the drop and the instantaneous volume of the drop) and surface tension was plotted as a function of average concentration (measured from change of volume of pendant drop) of CPC. But during evaporation instead of following equilibrium surface tension curve, the dynamic surface tension data (due to evaporation) were lower compared to equilibrium surface tension and followed a different curve (black circles, Figure 4.4), indicating higher adsorption of CPC to interface than would be expected at the average concentration.

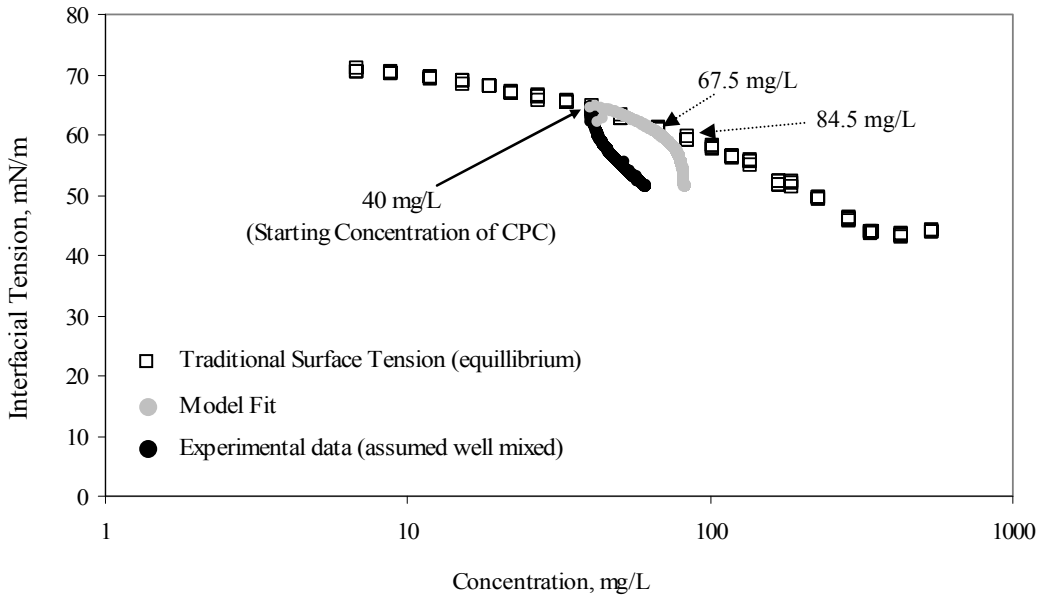

Figure 4.8: Interfacial tension of CPC at different concentration during evaporation [Molecular Diffusion Coefficient, D: $2x10^{-12}$ m^2/s]

Considering this experimental data (interfacial tension data), it was hypothesized that during evaporation, adsorption of CPC at the contracting air/water interface is rapid compared to diffusion of CPC to the solution. That means during evaporation, as volume decreased at every instant, a layer having concentration gradient (high to low from air/water surface to the well mixed core of the pendent drop) was developed due to slower diffusion of CPC away from the contracting surface compared with the rate of surface motion. By using the molecular diffusion coefficient, D ($2x10^{-12}$ m^2/s), the evaporation model #1 successfully able to model the experimental data to follow equilibrium surface tension curve up to certain concentration (67.5 mg/L) (Figure 4.8). After that, the interfacial tension dropped at a faster rate and after 84.5 mg/L, the interfacial tension dropped almost vertically to 51 mN/m. Figure 4.9 shows modeling of the three different concentration of CPC pendent drop having starting (equilibrium) surface tension data below CMC.

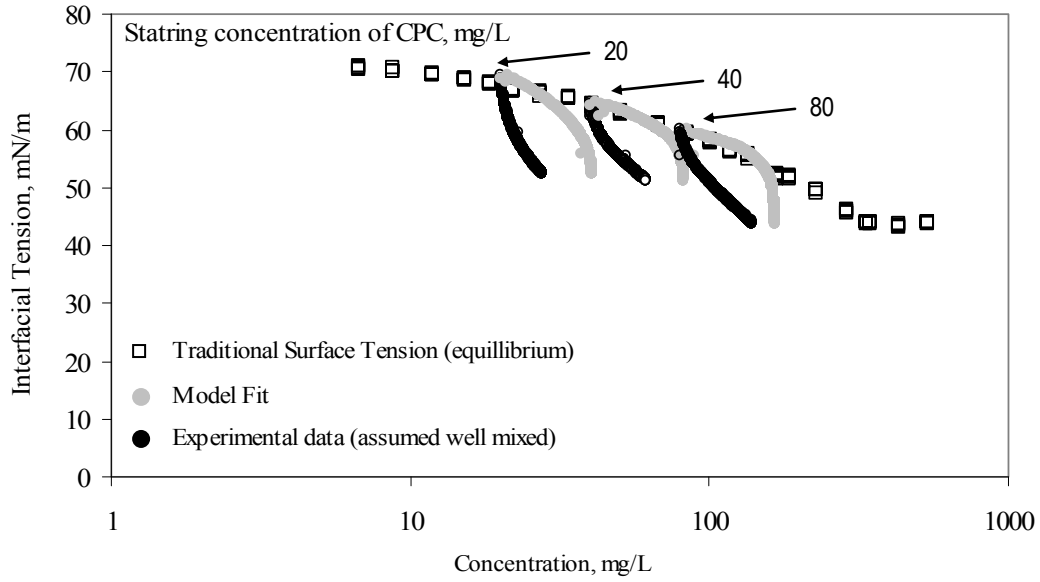

Figure 4.9: Interfacial tension of CPC at different concentration during Evaporation [Molecular Diffusion Coefficient, D: $2x10^{-12}$ m^2/s]. Three different initial concentration CPC solutions were used in the experiment.

For every initial concentration of CPC, the molecular diffusion coefficient ($D=2x10^{-12}$ m^2/s) was used to predict the concentration in the pendent drop at surface. All three concentrations show similar trends, the evaporation model #1 is able to match the traditional surface tension data to some extent and after that, a sudden drop of surface tension. Rate of volume change was pretty consistent for all three concentrations (0.4~.43 μL/min).

Figure 4.10 shows the application of the evaporation model #1 for the evaporation of a non ionic surfactant, NP15 at two different starting concentrations. A diffusion coefficient, $D = 1x10^{-11}$ m^2/s was used for both concentrations. In Figure 4.10, two traditional surface tension curves have shown (one measure by pendent drop method (4) and another measured by bubble method (4).)

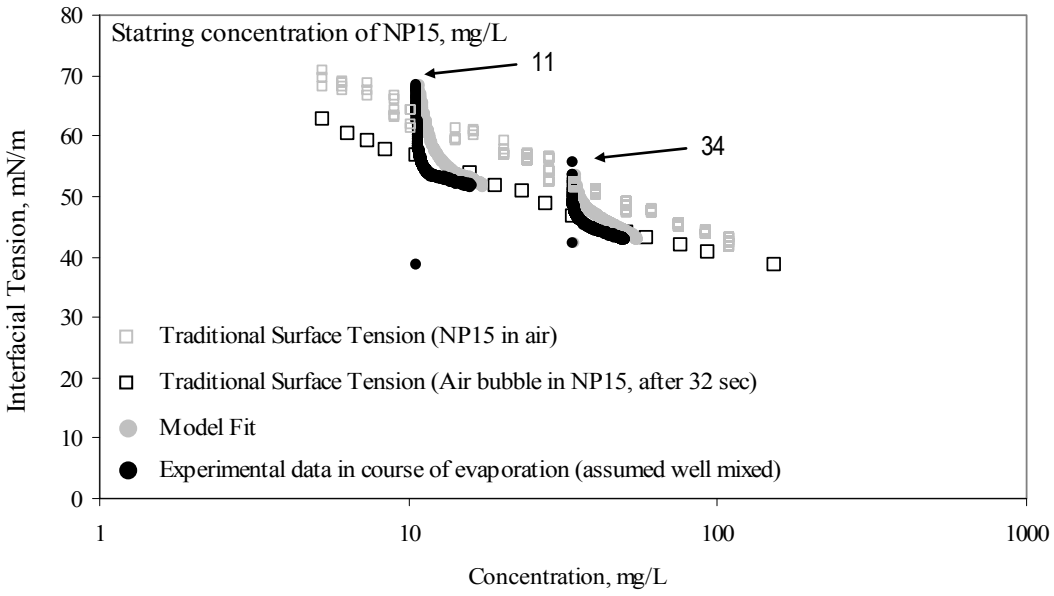

Figure 4.10: Interfacial tension of NP15 at different concentration during Evaporation [Diffusion Coefficient, D (considered for modeling): $1x10^{-11}$ m^2/s].

As explained in section 3.3 and Figure 3.12 it is safe to assume NP15 takes longer time to reach equilibrium surface/interfacial tension and traditional curve obtained by bubble method after 32 sec gives more reasonable equilibrium surface tension data for the purpose.

The starting surface tensions (just after evaporation started) were higher than the equilibrium surface tension (bubble method) and later, in the course of evaporation, the dynamic surface tension reduced and matched equilibrium surface tension. As for example in Figure 4.10 for initial concentration of 34 mg/L, starting surface tension was ~55 mN/m but later it reduced to ~47 mN/m and matched equilibrium surface tension (bubble method). A probable explanation to this scenario is, when a fresh surface of water formed, theoretically the surface tension should be ~72 mN/m and as surfactant starts to adsorb, surface tension decreases. At the beginning of the evaporation experiment, the image corresponding to 55 mN/m drop might not have sufficient amount of surfactant adsorbed to attain equilibrium surface tension (47 mN/m) and later, when adequate surfactant monomer adsorbed, the surface tension reduced to equilibrium surface tension. One important point to be noted: the diffusion coefficient ($1x10^{-11}$ m^2/s) used in case of NP15 is not very realistic, as the actual value is likely order of magnitude lower. Furthermore, the model could not fit the data very well.

Figure 4.11 shows the application of the evaporation model #2 for the evaporation of CPC. Same experimental data showed in Figure 4.7, 4.8 and 4.9 are used in this second model. Two different starting concentrations, 40 and 80 mg/L data was shown in figure 4.11. For both concentrations, the same diffusion coefficient ($2x10^{-12}$ m^2/s) as the previous model was used to calculate actual concentration at drop surface.

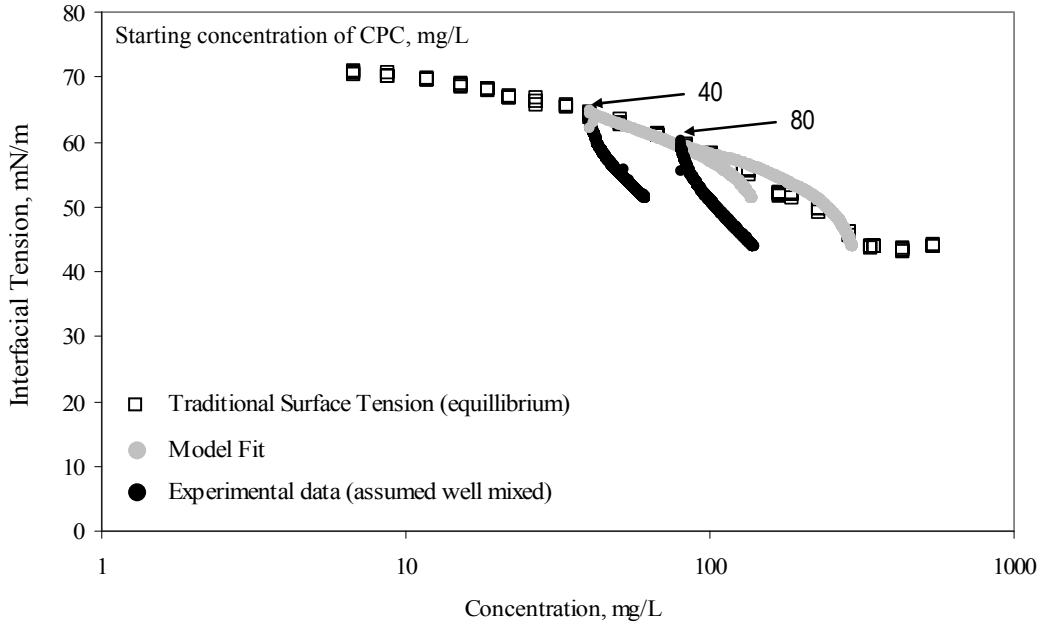

Figure 4.11: Interfacial tension of CPC at different concentration during Evaporation [Diffusion Coefficient, D (considered for modeling): $2x10^{-12}$ m^2/s]. Three different initial concentration CPC solutions were used in the experiment.

Unlike model #1, the model #2 successfully able to fit the experimental data with the traditional surface tension curve for the entire range. Although a little drift at the high concentration end is still evident for 40 mg/L (starting concentration) drop, compare to Figure 4.8, Figure 4.11 shows much better fit to the traditional curve.

Figure 4.12 shows the application of the model #2 for the evaporation of NP15. Like CPC, same experimental data showed in Figure 4.10 are used in this model. For both starting concentrations (11 mg/L and 34 mg/L), same diffusion coefficient, $1x10^{-11}$ m^2/s was used to model surface concentration.

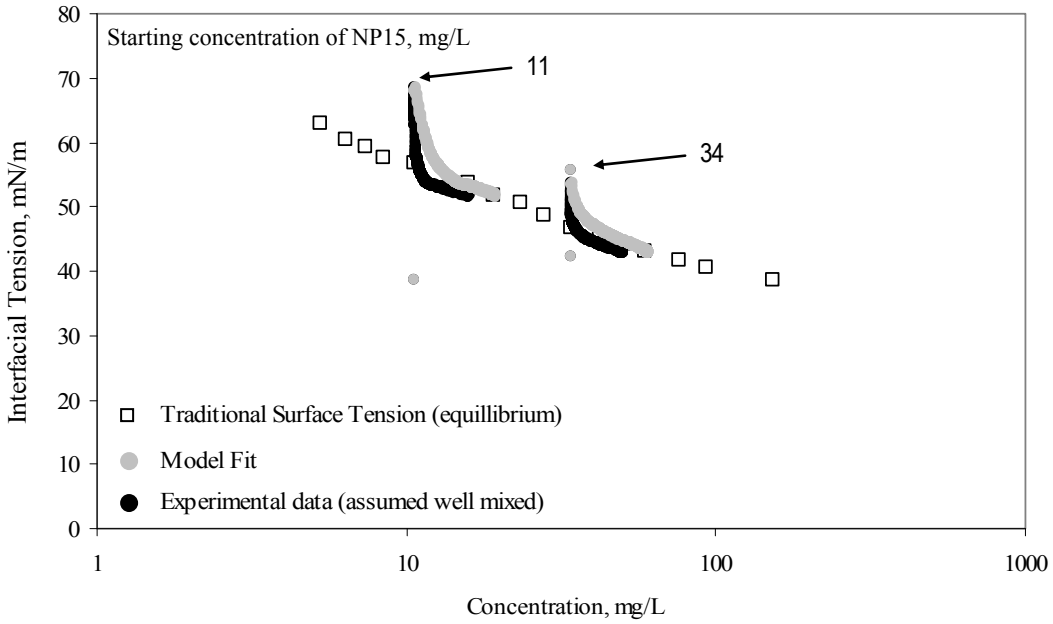

Figure 4.12: Interfacial tension of NP15 at different concentration during Evaporation [Diffusion Coefficient, D (considered for modeling): $1x10^{-11}$ m^2/s].

Important point to be noted: both of these models are first-cut efforts to model interfacial tension changes during evaporation. Results suggest that modeling diffusion can capture many of the feathers of interfacial tension change resulting from evaporation. However, more work is needed develop a more accurate numerical model to study the evaporation behavior of surfactant solution.

In order to examine the hypotheses underlying the evaporation models, the evaporation experiment was conducted in a closed cell to minimize evaporation. The optical cell was also saturated with moisture prior to start the evaporation to further slowing down the evaporation. If diffusion rate away from the surface is the limiting factor, then slowing evaporation should cause the dynamic surface tension curve based

on average concentration to closely match the traditional curve. Figure 4.13 shows the quantitative analysis of the evaporation of CPC pendant drop in a closed cell. From the figure it is evident that the average concentration of the drop hardly increased (from 80 mg/L to 81.2 mg/L) but the interfacial tension still does not match with the traditional surface tension curve. Instead the surface tension decreased sharply from 60.7mN/m to 54.7mN/m. In other words the surface concentration is still much higher than the average concentration of the drop.

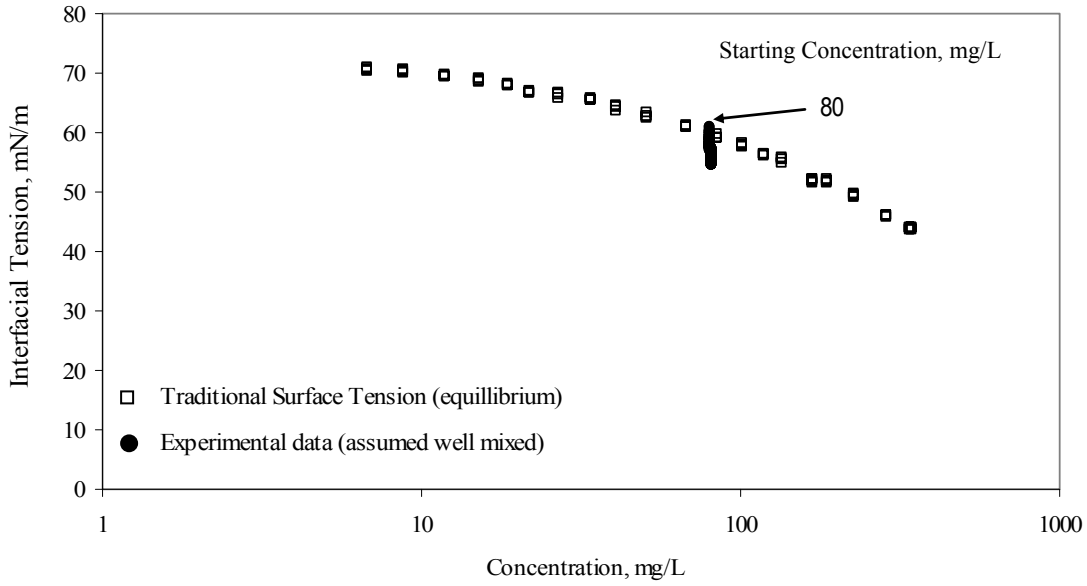

Figure 4.13: Interfacial tension of CPC at different concentration during evaporation in a closed cell

Further study including diffusion of surfactant in complete absence of evaporation is required to get some more insight of the adsorption scenario of surfactant.

4.4. CONCLUSIONS

Diffusion plays a key role in surface/interfacial tension modification of surface/interfaces. Results from evaporation experiments are quite consistent with the results from dilution experiments (as discussed in chapter 3). Like dilution experiments, modeling of CPC evaporation data shows that surface/interfacial tension modification of CPC is diffusion rate limiting. By adjusting diffusion rate, dynamic surface/interfacial tension can be approached to equilibrium surface tension.

Modeling of NP15 evaporation data shows similar result found in dilution experiments (Instead of fitting to instantaneous surface tension curve, the model fits to the traditional curve generated after adsorbing for 32 seconds). So traditional curve obtained by bubble method (after adsorbing 32 seconds at each concentration) was used to model evaporation data. So in case of nonionic surfactant, NP15, it can be assumed that initially the equilibration was adsorption rate limiting and after certain time (in case of NP15 it was 32 seconds) the surface/interfacial tension modification of NP15 becomes diffusion rate limiting. Further experiments with other nonionic surfactants and anionic surfactants are required to have a better understanding of the dynamics of interface equilibration processes. This study can also become the basis of the development of a rapid method of surface/interfacial tension curve for different types of surfactant.

CHAPTER 5

CONCLUSIONS

5.1. CONCLUSIONS

The research work presented here examines the dynamics of surface equilibration process of organic liquids and corresponding implication for changes of wettability. Although surface/interface equilibration and wettability are two different processes, they are closely related to each other when applied to organic liquids. Three different types of experiments were designed: (i) dissolution of DNAPL sessile drop in water or low concentration surfactant solution, (ii) dilution of surfactant pendant drop in air and (iii) evaporation of surfactant pendent drop in air.

5.1.1. *Dynamics of change of Wettability of Organic Liquids*

When organic liquid comes in contact with ground water in the subsurface, organic liquids dissolves in water, and water dissolves in organic liquids, until the two phases are in equilibrium. This mutual saturation process leads to a change in interfacial tension and wettability (contact angle) of organic liquids.

Dissolution of two different DNAPLs (TCE and PCE) in water and in presence of low concentration surfactants (CTAB, SDBS and NP9) was examined to understand the change of wettability. It was observed that dissolving drops tend to retain their initial contact diameters during dissolution for a wide range of systems; i.e., the original footprint of the drop on the surface does not change during dissolution. Considering the experimental results, a numerical model was developed to model the effect of dissolution

on contact angle if contact diameter is held constant. The model was based on solution of Bashforth-Adams equation, which describes the shape of an axisymmetric drop of a particular interfacial tension and density difference from the surrounding fluid. The major findings from the experiments are:

- Dissolution causes contact angle of TCE and PCE to reduce well below receding contact angle.
- The interfacial tension shows an initial decrease (perhaps because of the mutual saturation of interfacial regions of the two phases (Water/TCE or Water/PCE)) and then shows a gradual decrease with the decrease of drop volume over the course of dissolution.
- The contact angle of TCE initially increased followed by a gradual decrease over the course of dissolution
- While contact angle of DNAPLs were gradually decreasing and contact diameters were pinned over the course of dissolution in most of the systems, there were some occasional slips of contact angle and contact diameter observed in some dissolution experiments.

The dissolution model was used to generate the predicted drop profile over time for a dissolving drop with a fixed contact diameter, as well as the predicted contact angle as a function of volume during dissolution.

DNAPL drops are highly unlikely to be positioned on flat surface (as examined in this work) in the subsurface aquifer system. More likely DNAPLs are to be entrapped in

the aquifer pores and initially behave as non wetting phase. Over the course of dissolution, if contact angle between DNAPL and aquifer surface reduces (as observed in this work), DNAPL will gradually change into wetting phase. If the contact angle approaches zero, then additional hydrostatic force will be needed to mobilize the DNAPLs. This scenario may lead to flow bypassing the smaller pores and cause longer remediation time.

5.1.2. *Dynamics of interface equilibration processes*

Dynamic surface/interfacial tension of surfactant solution has been studied and compared with the equilibrium surface tension to understand the dynamics of mixing and surface/interfacial adsorption. The dynamics of adsorption vs. diffusion/mixing plays a key role in interface equilibration process by modifying surface/interfacial tension.

The surface/interface equilibration of surfactant solution has been examined in the course of dilution and evaporation. In dilution experiments, water was pumped in high concentration surfactant pendent drop and change of surface/interfacial tension was observed in the course of dilution. In evaporation experiments, surfactant pendent drop were formed, held in the air to evaporate and change of surface/interfacial tension was observed in the course of evaporation. The major findings from the experiments are:

- Dynamic surface/interfacial tension of surfactant pendent drop is lower than the equilibrium surface tension in the course of both dilution and evaporation.

- For CPC (cationic surfactant), adsorption of surfactant at the surface was found to be faster compared to diffusion/mixing in the course of both dilution and evaporation.

- For SOBS (anionic surfactant), adsorption of surfactant at the surface was found to be faster compared to diffusion/mixing in the course of dilution.

- NP15 takes longer time to adsorb and attain equilibrium surface tension than the other surfactant solutions.

5.2. RECOMMENDATIONS FOR FUTURE WORK

Additional related studies which could help to strengthen and expand the findings of the work presented here include:

- Dissolution experiments involving larger (volume) PCE drops by using a flow-through system.

- Dissolution of DNAPLs in high concentration surfactant solution. One preliminary experiment was conducted with TCE in a high concentration SDBS solution (data not shown) showed some slipping in the drop footprint with dissolution, but nevertheless found a continuous decrease in contact angle with dissolution.

- Experiments examining dissolution of DNAPLs from capillaries, and the effects on corresponding forces needed to cause them to drain. These

experiments would provide useful insight into remediation of DNAPLs entrapped in small pores of aquifer material.

- Diffusion of surfactant in complete absence of evaporation. These experiments may give some more insight of adsorption vs. diffusion scenario of surfactant.

- Developing a numerical model for evaporation of surfactant using spherical equation for diffusion instead of 1D diffusion equation to better understand the adsorption of surfactant in the course of evaporation.

REFERENCES

(1) Ferri, J. K. and Stebe, K. J., **"**Which surfactants reduce surface tension faster? A scaling argument for diffusion-controlled adsorption", *Advances in Colloid and Interface Science*, 85 (1), pp. 61-97, 2000.

(2) Rosen, J. M. *Surfactants and Interfacial Phenomena*, 2nd ed.; Wiley: New York, 1989.

(3) Tadros, T.F., *Applied Surfactants: Principles and Applications*, Wiley-VCH, Weinheim, 2005, ISBN 3-527-30629-3.

(4) Adamson, A. W.; Gast, A. P. *Physical Chemistry of Surfaces*, 6th ed.; Wiley: New York, 1997.

(5) Heimenz, P. C.; Rajagopalan, R. *Principles of Colloid and Surface Chemistry*, 3rd ed.; Marcel Dekker: New York, 1997.

(6) Eastoe, J., and Dalton, J.S., "Dynamic surface tension and adsorption mechanisms of surfactants at the air-water interface," *Advances in Colloid and Interface Science*, 85 pp. 103-144, 2000.

(7) Yang, C. and Gu, Y., "Modeling of the adsorption kinetics of surfactants at the liquid-fluid interface of a pendant drop," *Langmuir*, 20(6), pp. 2503-25011, 2004.

(8) Clint, J.H., *Surfactant Aggregation,* Blackie & Son Ltd., 1992, ISBN 0-216-92905-9.

(9) Fainerman, V. B., Miller, R., and Joos, P., "The measurement of dynamic surface tension by the maximum bubble pressure method," *Colloid and Polymer Science*, 272 (6), pp. 731-739, 1994.

(10) Miller, R.; Zholob, S. A.; Makievski, A. V.; Joos, P.; Fainerman, V. B.; "Remarks on the Interpretation of Data from the Dynamic Drop Volume Method," *Langmuir*, 13(21), pp. 5663-5668, 1997.

(11) Rotenberg, Y.; Boruvka, L.; Neumann, A. W.; "Determination of surface tension and contact angle from the shapes of axisymmetric fluid interfaces," *Journal of Colloid and Interface Science*, 93(1), pp. 169-183, 1983.

(12) Faour, G.; Grimaldi, M.; Richou, J.; Bois, A; "Real-time pendant drop tensiometer using image processing with interfacial area and interfacial tension control capabilities," *Journal of Colloid and Interface Science*, 181(2), pp. 385-392, 1996.

(13) Rio, O. I. D.; Neumann, A. W. Axisymmetric drop shape analysis: Computational methods for the measurement of interfacial properties from the shape and

dimensions of pendant and sessile drops. *J. Colloid Interface Sci.* 1997, *196*, 136-147.

(14) Ward, A. F. H.; Tordai, L; "Time dependence of boundary tensions of solutions. I. The role of diffusion in time effects," *Journal of Chemical Physics*, 14, pp. 453-461, 1946.

(15) Fainerman, V. B.; Makievski, A. V.; Miller, R.., "The analysis of dynamic surface tension of sodium alkyl sulfate solutions, based on asymptotic equations of adsorption kinetic theory," *Colloids and Surfaces, A: Physicochemical and Engineering Aspects*, 87(1), pp. 61-75, 1994.

(16) Liu, J, and Messow, U., "Diffusion – controlled adsorption kinetics at the air/solution interface," *Colloid and Polymer Science*, 278, pp. 124-129, 2000.

(17) Bear, J. *Dynamics of Fluids in Porous Media*; Dover: New York, 1972.

(18) Bedient, P. B.; Rifai, H. S.; Newell, C. J. *Ground Water Contamination: Transport and Remediation*, 2nd ed.; Prentice Hall: Upper Saddle River, NJ, 1999.

(19) Mackey, D. M.; Cherry, J. A. Groundwater contamination: Pumpand-treat remediation. *Environ. Sci. Technol.* 1989, *23*, 630-636.

(20) Mercer, J. W.; Cohen, R. M. A review of immiscible fluids in the subsurface: Properties, models, characterization and remediation. *J. Contam. Hydrol.* 1990, *6*, 107-163.

(21) U.S. Environmental Protection Agency. *Evaluation of the Likelihood of DNAPL Presence and NPL Sites*; Washington, DC, 1993; OSWER 9355.4-13, EPA/540-R-93-073.

(22) U.S. Environmental Protection Agency. *Common Chemicals found at Superfund Sites* (EPA/540-R-94-044); Office of Emergency and Remedial Response, Washington, DC, 1994.

(23) Kueper, B. H.; Redman, D.; Starr, R. C.; Reitsma, S.; Mah, M. A field experiment to study the behavior of tetrachloroethylene below the water table: Spatial distribution of residualandpooled DNAPL. *Ground Water* 1993, *31*, 756-766.

(24) Powers, S. E.; Anckner, W. H.; Seacord, T. F. Wettability of NAPLcontaminated sands. *J. Environ. Eng.* 1996, *122*, 889-896.

(25) Bradford, S.; Vendlinski, R.; Abriola, L. The entrapment and long-term dissolution of tetrachloroethylene in fractional wettability porous media. *Water Resour. Res.* 1999, *35*, 2955-2964.

(26) Warr, G. G.; Scales, P.; Grieser, F.; Aston, J. R.; Furlong, D. R.; Healey, T. W. Polydisperse non-ionic surfactants, their solution chemistry and effect on the

wettability of solid surfaces. In *Surfactants in Solution*; Mittal, K. L., Lindman, B., Eds.; Plenum: New York, 1984; pp 1329-1338.

(27) Rixey, W. G.; Fuerstenau, D. W. The Young equation and the effect of surfactants on the wettability of minerals. *Colloids Surf., A* 1994, *88*, 75-89.

(28) Lord, D.; Demond, A. H.; Salezadeh, A.; Hayes, K. F. The relationship between solution chemistry and organic liquid migration in the subsurface 2. Capillary pressure-saturation. *Environ. Sci. Technol.* 1997, *31*, 2052-2058.

(29) Barranco, F. T.; Dawson, H. E.; Christener, J. M.; Honeyman, B. D. Influence of aqueouspHand ionic strength on the wettability of quartz in the presence of dense nonaqueous-phase liquids. *Environ. Sci. Technol.* 1997, *31*, 676-681.

(30) Starkweather, B. A.; Zhang, X.; Counce, R. M. An experimental study of the chance in contact angle of an oil on a solid surface. *Ind. Eng. Chem. Res.* 2000, *39*, 362-366.

(31) Rowe, A. W.; Counce, R. M.; Morton, S. A.; Hu, M. Z.-C.; DePaoli, D. W. Oil detachment from solid surfaces in aqueous surfactant solutions as a function of pH. *Ind. Eng. Chem. Res.* 2002, *41*, 1787-1795.

(32) Dekker, T. J.; Abriola, L. M.; The influence of field-scale heterogeneity on the infiltration and entrapment of dense nonaqueous phase liquids in saturated formations. *J. Contam. Hydrol.* 2000A, *42*, 187-218.

(33) Cheng, P. W. P. Automation of Axisymmetric Drop Shape Analysis using Digital Image Processing. Ph.D. Dissertation, University of Toronto, 1990.

(34) Cheng, P.; Li, D.; Boruvka, L.; Rotenberg, Y.; Neumann, A. W. Automation of axisymmetric drop shape analysis for measurements of interfacial tensions and contact angles. *Colloids Surf.* 1990, *43*, 151-167.

(35) Cheng, P.; Neumann, A. W. Computational evaluation of axisymmetric drop shape analysis-profile (ADSA-P). *Colloids Surf.* 1992, *62*, 297-305.

(36) Press, W.; Flannery, B.; Teukolsky, S.; Vetterling, W. *Numerical Recipes in C*; Cambridge University Press: New York, 1988.

(37) Kwok, D.; Lam, C.; Li, A.; Leung, A.; Wu, R.; Mok, E.; Neumann, A. Measuring and interpreting contact angles: a complex issue. *Colloids Surf., A* 1998, *142*, 219-235.

(38) Demond, A. H.; Lindner, A. S. Estimation of interfacial tension between organic liquids and water. *Environ. Sci. Technol.* 1993, *27*, 2318-2331.

(39) Shiau, B. J.; Hasegawa, M. A.; Brammer, J. M.; Carter, T.; Goodspeed, M.; Harwell, J. H.; Sabatini, D. A.; Knox, R. C.; Szekeres, E. Field demonstration of

surfactant-enhancedDNAPL remediation: two case studies. In *Chlorinated Solvent and*

DNAPL Remediation: Innovative Strategies for Subsurface Cleanup; Henry, S. M., Warner, S. D., Eds.; American Chemical Society Symposium Series 837; American Chemical Society: Washington, DC, 2003; pp 51-72.

(40) Taylor, T. P.; Pennell, K. D.; Abriola, L. M.; Dane, J. H. Surfactant enhanced recovery of tetrachloroethylene from a porous medium containing low permeability lenses 1. Experimental studies. *J. Contam. Hydrol.* 2001, *48*, 325-350.

(41) Chou, S. I.; Bae, J. H. Surfactant precipitation and redissolution in brine. *J. Colloid Interface Sci.* 1983, *96*, 192-203.

(42) Kibbey, T. C. G.; Hayes, K. F. A predictive numerical thermodynamic model of mixed nonionic surfactant sorption in natural systems. 2. Application to broadly distributed mixtures. *J. Colloid Interface Sci.* 1998, *197*, 210-220.

(43) Mohammad, O. I., and Kibbey, T.C.G., "Dissolution – Induced contact angle modification in dense nonaqueous phase liquid / water systems", *Environmental Science and Technology*, 39 (6), 1698 -1706, 2005.

(44) Amirfazli, A.; Hanig, S.; Muller, A.; Neumann, A. W. Measurements of line tension for solid-liquid-vapor systems using drop size dependence of contact angles and its correlation with solidliquid interfacial tension. *Langmuir* **2000**, *16*, 2024-2031.

(45) Amirfazli, A.; Kwok, D. Y.; Gaydos, J.; Neumann, A. W. Line tension measurements through drop size dependence of contact angle. *J. Colloid Interface Sci.* **1998**, *205*, 1-11.

(46) Gu, Y. Drop size dependence of contact angles of oil drops on a solid surface in water. *Colloids Surf., A* 2001, *181*, 215-224.

(47) Lunkenheimer, K., Wienskol, G., and Prosser, A.J., "Automated high performance purification of surfactant solutions: Study of convective-enhanced adsorption," *Langmuir*, 20, 5738-5744, 2004.

(48) Lunkenheimer, K., Pergande, H.J., and Krüger, H., "Apparatus for programmed high-performance purification of surfactant solutions," *American Institute of Physics*, 58, 2313-2316, 1987.

(49) Crank, J., *The Mathematics of Diffusion*, 2nd edition; Oxford University Press Inc., NY, 1975.

(50) Helmy, A.K., Bussetti, S.G.D., and Ferreiro, E.A., **"**The water–silicas interfacial interaction energies," *Applied Surface Science*, 253, 6878–6882, 2007.